



HAL
open science

The Stardalur magnetic anomaly revisited – new insights into a complex cooling and alteration history

C. Vahle, A. Kontny, H.P. Gunnlaugsson, L. Kristjansson

► To cite this version:

C. Vahle, A. Kontny, H.P. Gunnlaugsson, L. Kristjansson. The Stardalur magnetic anomaly revisited – new insights into a complex cooling and alteration history. *Physics of the Earth and Planetary Interiors*, 2007, 164 (3-4), pp.119. 10.1016/j.pepi.2007.06.004 . hal-00532117

HAL Id: hal-00532117

<https://hal.science/hal-00532117>

Submitted on 4 Nov 2010

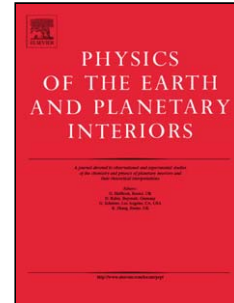
HAL is a multi-disciplinary open access archive for the deposit and dissemination of scientific research documents, whether they are published or not. The documents may come from teaching and research institutions in France or abroad, or from public or private research centers.

L'archive ouverte pluridisciplinaire **HAL**, est destinée au dépôt et à la diffusion de documents scientifiques de niveau recherche, publiés ou non, émanant des établissements d'enseignement et de recherche français ou étrangers, des laboratoires publics ou privés.

Accepted Manuscript

Title: The Stardalur magnetic anomaly revisited – new insights into a complex cooling and alteration history

Authors: C. Vahle, A. Kontny, H.P. Gunnlaugsson, L. Kristjansson



PII: S0031-9201(07)00134-3
DOI: doi:10.1016/j.pepi.2007.06.004
Reference: PEPI 4843

To appear in: *Physics of the Earth and Planetary Interiors*

Received date: 21-12-2006
Revised date: 21-5-2007
Accepted date: 14-6-2007

Please cite this article as: Vahle, C., Kontny, A., Gunnlaugsson, H.P., Kristjansson, L., The Stardalur magnetic anomaly revisited – new insights into a complex cooling and alteration history, *Physics of the Earth and Planetary Interiors* (2007), doi:10.1016/j.pepi.2007.06.004

This is a PDF file of an unedited manuscript that has been accepted for publication. As a service to our customers we are providing this early version of the manuscript. The manuscript will undergo copyediting, typesetting, and review of the resulting proof before it is published in its final form. Please note that during the production process errors may be discovered which could affect the content, and all legal disclaimers that apply to the journal pertain.

1 **The Stardalur magnetic anomaly revisited – new insights into a complex cooling and**
2 **alteration history**

3
4 C. Vahle ^{*a}, A. Kontny ^a, H.P. Gunnlaugsson ^b, L. Kristjansson ^c

5
6 ^a Geologisch-Paläontologisches Institut, Ruprecht-Karls-University Heidelberg, INF 234, D-
7 69120 Heidelberg, Germany

8 ^b Institute of Physics and Astronomy, Aarhus University, Ny Munkegade, DK-8000 Århus C,
9 Denmark

10 ^c Institute of Earth Sciences, University of Iceland, Sturlugata 7, Askja, IS-101 Reykjavík,
11 Iceland

12
13 To be submitted to Physics of the Earth and Planetary Interiors

14
15 **Abstract**

16 This study provides new rock magnetic and magneto-mineralogical data including Mössbauer
17 spectroscopy of basaltic drill cores from the Stardalur volcanic complex, Iceland, in order to
18 better understand the strong magnetic anomaly, which is caused by an extraordinary high
19 natural remanent magnetization (NRM). NRM and magnetic susceptibility (χ) display a
20 positive linear correlation ($R^2 = 0.81$) and reach very high values up to 121 A/m and $148 \cdot 10^{-3}$
21 SI. Although a Curie temperature of 580 °C and a Verwey transition at about -160 °C is
22 indicative of magnetite, χ -T heating experiments in argon and air atmosphere and thermal
23 demagnetization measurements of NRM revealed a slight cation-deficiency. According to
24 induced remanent magnetization experiments the remanence is carried solely by this low
25 coercive phase. Minor titanomaghemite with a T_C at about 340 °C only occurs in samples
26 with larger oxide grains (20 – 80 μm). High vesicle abundances and the exsolution texture of
27 Fe-Ti oxides suggest subaerial extrusion of the lava. A high oxygen fugacity (probably above
28 the NNO buffer) and a low Ti/(Ti+Fe) ratio of the basaltic melt are suggested as a
29 precondition for high concentration of magnetic minerals and therefore high primary TRM.
30 During high temperature oxidation, ilmenite exsolution-lamellae, developed in

* corresponding author

31 titanomagnetite, and symplectic magnetite (+ pyroxene) formed by the breakdown of olivine.
32 This secondary magnetite, grown at temperatures above the Curie temperature, increases the
33 primary TRM. Early stage hydrothermal alteration (below about 375 °C) led to
34 maghemitization of (titano)magnetite, clearly indicated by shrinkage cracks and irreversible
35 χ -T curves. During later stage hydrothermal alteration NRM intensity increased slightly due
36 to the growth of secondary magnetite at lower temperatures (about 250 – 300 °C). This
37 hydrothermally formed magnetite acquired only a low CRM but increased magnetic
38 susceptibility significantly. According to our results it is suggested, that hydrothermal
39 alteration does not necessarily lower remanent magnetization, but contributes to an increase in
40 magnetization. The interplay of the three factors melt composition, small grain sizes of
41 secondary magnetite due to decomposition of silicates and new formation under hydrothermal
42 conditions caused the strong magnetic anomaly at the surface.

43

44 **Keywords:** magnetic anomaly; rock magnetism; NRM; magnetite; maghemite; basalt
45 alteration

46

47 **1. Introduction**

48 Aeromagnetic surveys of Iceland have revealed different types of magnetic anomalies.
49 Mainly, they are aligned subparallel to currently active or extinct spreading zones. The
50 resulting magnetic lineations are related to tilted blocks and/or changes in magnetic polarity
51 (Jonsson et al., 1991). Additionally, several localized magnetic anomalies of 5 – 10 km in size
52 are associated with volcanic centers. Some have high magnetic intensity (positive anomaly in
53 a negatively polarized area), others show magnetic lows (negative anomaly surrounded by
54 strong positive anomaly), like in the Krafla-Namafjall area (Fig. 1a). The latter type seems to
55 be related to hydrothermal activity in geothermal fields.

56 The strongest of the localized positive magnetic anomalies is observed at the Stardalur
57 volcanic complex, 20 km NE of Reykjavik (Fig. 1, Fridleifsson and Kristjansson, 1972).
58 According to unpublished data from Th. Sigurgeirsson from an aeromagnetic survey at 100 –
59 200 m above ground, the maximum field of the Stardalur magnetic anomaly is 59 μ T,
60 whereas the neighboring area gives only 51 μ T. The Stardalur volcanic complex is of Olduvai
61 age (~ 1.8 Ma) and consists of a 6.5 km caldera, cone-sheet swarm, sills and a laccolithic
62 body. At the northern rim of the caldera, intensive fracturing enabled hydrothermal activity.

63 The volcanic complex is embedded into thick successions of basaltic lava flows of Quaternary
64 age, intercalated with hyaloclastite ridges and glacial deposits (Fridleifsson, 1973).

65 In the years 1969-70, a 200 m deep borehole was drilled into the area of maximum field
66 intensity of the Stardalur magnetic anomaly. A first rock magnetic characterization of these
67 drill cores was done by Fridleifsson and Kristjansson (1972). The average natural remanent
68 magnetization (NRM) was 61 A/m. This is about 10 times higher than the average of other
69 Icelandic Quaternary basalts (Kristjansson, 1970). From thermomagnetic measurements done
70 in air, the authors found magnetite resulting from high temperature oxidized titanomagnetite,
71 which is in some cases subsequently oxidized to maghemite. Due to stable NRM directions
72 and no time dependence they excluded a strong viscous overprint. Furthermore, the small
73 scattering of the NRM inclination ($81 \pm 4^\circ$) pointed to a short time interval of lava
74 emplacement (~ 2000 years). Based on saturation remanence and susceptibility data,
75 Fridleifsson and Kristjansson (1972) estimated the magnetite content to be 2.5 vol.%. They
76 concluded this high magnetite content to be one reason for the unusually strong magnetic
77 anomaly. Additionally, they assumed a high paleomagnetic field intensity of $93 \pm 6 \mu\text{T}$ at the
78 time of NRM acquisition (actual Earth magnetic field at Stardalur is $52 \mu\text{T}$, IGRF-10). It was
79 also suggested, that rather small grain sizes resulting from rapid cooling or oxidation
80 contribute to high NRM.

81 Helgason et al. (1990) inferred similar conclusions and suggested an additional self-
82 amplification effect of the magnetic field due to hydrothermal reheating from below. The
83 oxidized titanomagnetite (magnetite with Curie temperature of 580°C) shows still
84 ferromagnetic behavior despite elevated temperatures due to hydrothermal heating and
85 therefore increases the local magnetic field. According to Mössbauer spectra they found
86 neither maghemite nor Ti in the magnetic phase, only pure and homogeneous magnetite. But
87 Helgason et al. (1990) stated already “that the key of the riddle lies in the alteration process”.

88 Using Mössbauer spectra and scanning electron microscopy (SEM) Gunnlaugsson et al.
89 (2006) have shown the influence of oxidized olivine on magnetic properties of olivine basalt.
90 According to their study, submicroscopic single-domain magnetite, which formed by
91 oxidation of olivine, increases NRM. Therefore the NRM of basalts containing olivine could
92 be an order of magnitude higher than that of olivine-free basalts. Furthermore, Stardalur
93 samples have been found to have a rather high Fe-content of ~ 12 wt.% Fe (Steinthorsson and
94 Sigvaldason, 1971), with an unusually large proportion of Fe situated in magnetite (about 30

95 % of the area of the Mössbauer spectra, 5 – 10 % is more usual; Helgason et al., 1990;
96 Gunnlaugsson et al., 2003).

97 According to these previous studies following factors seem to account for the unusually high
98 magnetizations of the Stardalur rocks: 1) small grain size, 2) high temperature oxidized
99 titanomagnetite, resulting in almost pure magnetite, 3) magnetite oxidized from olivine and 4)
100 higher (local) paleomagnetic field intensity. Although it seems that probably all of these
101 factors contribute, the geological processes that led to the anomalously high magnetization of
102 the Stardalur rocks are not fully understood. Although Mössbauer studies revealed pure
103 magnetite as carrier of the magnetic properties (Helgason et al., 1990; Gunnlaugsson et al.,
104 2003, 2006) it is not fully clear up to now how the magnetite has actually formed and how the
105 textural relations are. Therefore, we combined rock magnetic and magneto-mineralogical
106 methods, in addition to some thermomagnetic experiments, to find further clues to this
107 extraordinary high magnetization. A better understanding of the Stardalur anomaly may be an
108 analogue for extraterrestrial magnetic anomalies, as e.g. observed on Mars, where strong
109 crustal anomalies are attributed to a high crustal remanence (e.g. Acuña et al., 1999). Models
110 suggest magnetic rocks of tenths of km thickness with remanent magnetization up to ~ 20
111 A/m (Purucker et al., 2000).

112

113 **2. Sample material and methods**

114 We investigated drill cores of the 200 m deep Stardalur borehole (Fig. 1b) drilled in the years
115 1969-70 (see above). The drill core revealed about 45 m of fresh olivine tholeiitic lava flows
116 and tuffs with low magnetic intensity. Below that depth until at least 140 m, strongly
117 magnetic early Quaternary lavas follow (Fridleifsson and Kristjansson, 1972). Between 35
118 and 143 m we measured magnetic susceptibility on full cores (Fig. 2) using a hand-held
119 kappameter (KT-5) from Geofyzika (now AGICO company). The measurement sensitivity is
120 $1 \cdot 10^{-5}$ SI based on frequency changes of the operating coil (10 kHz). The average distance
121 between single measurements was ~ 21 cm, whereas not the entire core was measured
122 because of missing sections. Based on the susceptibility profile we selected representative
123 samples, which reflect the observed susceptibility variations. From these samples, standard
124 cylindrical specimens (2.5 cm in diameter, 2.1 cm high) were prepared for different rock
125 magnetic investigations.

126 The magnetic susceptibility (χ) was measured in the laboratory on these specimens using
127 KLF-3 susceptometer of Geofyzika (now AGICO company) at 30 A/m and 2000 Hz. The

128 reliability and significance of routine susceptibility measurements on drill cores using a hand-
129 held kappameter were compared with laboratory measurements. This test gives a linear
130 relationship between both these methods with a high correlation coefficient ($R^2 = 0.99$, $n =$
131 11), whereas a general shift towards lower values for the hand-held kappameter
132 measurements can be observed ($y = 0.551 x - 0.497$). However, hand-held kappameter
133 measurements are used to reveal the pattern of magnetic susceptibility, but one must be aware
134 that the hand-held kappameter values are lower than those measured on standard cylindrical
135 specimens.

136 For the temperature dependence (-194 to 0 and from room temperature to 700 °C) of magnetic
137 susceptibility (χ -T) a KLY-4S kappabridge (working with 300 A/m and 875 Hz) combined
138 with a CS-L/CS-3 apparatus (AGICO company) was used. Heating/cooling rates range
139 between 3 - 4 and 11 - 14 °/min for the low temperature and high temperature run,
140 respectively. The high temperature runs were performed in an argon atmosphere in order to
141 avoid mineral reactions with oxygen during heating (flow rate of 110 ml/min). Some samples
142 were also measured in an air flow of the same rate. The raw data were corrected for the empty
143 cryostat/furnace and normalized to the susceptibility magnitude at 0 °C. The Néel or Curie
144 temperature (T_N or T_C) was determined graphically using the reciprocal susceptibility
145 according to the suggestions of Petrovsky and Kapicka (2005).

146 Measurements of remanent magnetization were done with a JR5A spinner magnetometer
147 (AGICO company). For stability tests, alternating field demagnetization (AF
148 demagnetization) was performed in peak fields up to 160 mT with a MI AFD 1.1 from
149 Magnon International. Stepwise thermal demagnetization up to 700 °C was done with the
150 Thermal Demagnetizer MMTD1 (Magnetic Measurements). Isothermal acquisition of
151 remanence (IRM) was measured using a commercial power supply unit connected with a coil
152 for fields up to ca. 90 mT. For selected samples IRM was applied at fields of 1.25 T with an
153 ASC Scientific Impulse Magnetizer (IM-10-30) and subsequent stepwise thermal
154 demagnetization was performed with an ASC Scientific Thermal Demagnetizer (TD-48) at
155 the Laboratory for Natural Magnetism, ETH-Zurich.

156 Oxide textures were characterized using reflected light and scanning electron microscopy in
157 backscatter mode (LEO 440). Mineral chemical data were obtained by electron microprobe
158 (CAMECA SX51) at the Institute of Mineralogy in Heidelberg. Standards used were periclase
159 (Mg), Al_2O_3 (Al), wollastonite (Si), TiO_2 (Ti), Cr_2O_3 (Cr), rhodonite (Mn), and hematite (Fe).

160 The raw data were corrected with the PAP algorithm of Pouchou and Pichoir (1984). An
161 acceleration voltage of 15 kV and a sample current of 20 nA were used.

162 Mössbauer spectra (done at the Institute of Physics and Astronomy of Aarhus University)
163 were recorded in transmission geometry at room temperature using 10 – 25 mCi $^{57}\text{Co}:\text{Rh}$
164 sources mounted on conventional drive systems. Isomer shifts (δ) and velocity are given
165 relative to the centre of the spectrum of $\alpha\text{-Fe}$.

166

167 **3. Results and interpretation**

168 Table 1 summarizes the rock magnetic parameters from the basaltic samples marked in Fig. 2.
169 The magnetic susceptibility pattern agrees quite well with lithological boundaries indicating
170 changes in cooling and alteration history. Natural remanent magnetization (NRM) versus
171 magnetic susceptibility (χ) of all specimens displays a positive linear correlation with $R^2 =$
172 0.81 (Fig. 3). NRM and χ reach very high values up to 121 A/m and $148 * 10^{-3}$ SI,
173 respectively. These high values suggest a high content of opaque minerals. A positive
174 correlation between the NRM and the estimated volume percent of the opaque minerals of
175 some polished sections (see below) confirms this assumption ($R^2 = 0.69$; $n = 7$). An even
176 better correlation with $R^2 = 0.75$ has been found between magnetic susceptibility and the
177 volume percentage of the opaque minerals.

178 Average values calculated for the strongly magnetic samples below 43 m are 62.6 ± 23.8 A/m
179 and $82.4 \pm 24.4 * 10^{-3}$ SI, respectively. These values fit quite well to the average NRM
180 intensity of 61 A/m for the Stardalur rocks given by Fridleifsson and Kristjansson (1972). A
181 comparison with NRM intensities and susceptibilities of other Quaternary Icelandic rocks
182 (about 10 times less magnetic, see Kristjansson, 1970) and of own unpublished data from
183 surface rocks of the Reykjanes peninsula (13.8 ± 6.2 A/m and $10.2 \pm 4.0 * 10^{-3}$ SI; recent lava
184 flows from fissure eruptions, shield volcanoes and pillow lava, all younger than 20000 years)
185 emphasizes the unusually high values for the Stardalur basalts. The Königsberger ratio, Q-
186 factor (ratio between remanent and induced magnetization), ranges between 7.5 and 30.4,
187 clearly indicating the predominance of remanent magnetization over induced magnetization.
188 Component analyses revealed only one stable characteristic remanence direction contributing
189 to the NRM. In the following sections, we give a rock magnetic and magneto-mineralogical
190 characterization to better understand the nature of this extraordinary magnetic behavior.

191

192 *3.1 Microscopic observations*

193 According to the lithological descriptions given in Fridleifsson and Tomasson (1972) the
194 units below about 45 m are altered olivine tholeiitic basalt. In the lower part of this section at
195 ~ 140 m depth, zeolite, montmorillonite and chlorite are reported. Based on our own
196 macroscopic observations the main part of the core from 44 down to 144 m consists of
197 differently strong altered fine-grained basalts with local carbonate and quartz fillings along
198 cracks and veins. Two breccia zones at 81 and 93 m, respectively, intercalate these basalts
199 (see Fig. 2). In the lowermost part (ST138.1) many vesicles (about 15 vol.%) with a diameter
200 of 1 – 5 mm point to subaerial extrusion of the lava. These vesicles are filled with white and
201 green minerals, probably the above described zeolite, montmorillonite and chlorite.

202 According to microscopic observations, the main silicates are subhedral (200 – 500 μm) or
203 columnar (~ 600 μm) clinopyroxene (augite or pigeonite, when in groundmass: 20 – 30 μm in
204 size) and plagioclase laths (60 – 800 μm in size). No olivine is observed, but in some samples
205 altered areas of 60 – 300 μm in size are found consisting of phyllosilicates (predominantly
206 chlorite), which could have been former olivine. According to their brown and greenish color,
207 some of these altered areas could be iddingsite (submicroscopic mélange of goethite, chlorite
208 and phyllosilicates), a low to intermediate temperature alteration product of olivine (Baker
209 and Haggerty, 1967). But also symplectic magnetite has been observed at some places (Fig.
210 4a), which is assumed to be a high temperature oxidation product of olivine. Based on heating
211 experiments of olivine basalt from different localities, Haggerty and Baker (1967) stated that
212 olivine oxidizes to magnetite + enstatite or hematite + forsterite depending on temperature
213 and oxygen fugacity.

214 Additionally to clinopyroxene and plagioclase, opaque minerals, carbonate, quartz and
215 chlorite occur in the Stardalur drill cores. Following opaque minerals have been identified:

- 216 - titanomagnetite: dendritic, cruciform, skeletal to euhedral grains, < 1 μm and up to 130
217 μm in size
- 218 - ilmenohematite: elongated skeletal to subhedral grains of 12 – 100 μm
- 219 - titanite: as alteration product of ilmenohematite and titanomagnetite
- 220 - sulfide phases: pyrite and chalcopyrite, subhedral grains up to 300 μm
- 221 - magnetite: net-like replacement products and vein fillings

222 The total abundance of the opaque minerals was estimated from thin section observations and
223 ranges between 6 and 15 vol.% (see Table 1). The opaque mineral assemblage is strongly

224 dominated by titanomagnetite, which has been proved by the application of a ferrofluid (see
225 e.g. Kletetschka and Kontny, 2005). Because the ferrofluid covers only magnetic phases like
226 titanomagnetite and magnetite, the coating with ferrofluid enables the discrimination of e.g.
227 ilmenite and magnetite. Ilmenohematite and especially titanomagnetite show different
228 textures and grain size populations, indicating different cooling and crystallization histories of
229 the basalts. Almost all titanomagnetite shows ilmenite exsolution-lamellae, resulting from
230 high temperature oxidation (Fig. 4b). Some ilmenohematite shows lenses of rutile and
231 probably hematite spots. In some cases sandwich-types are present. These textures are in
232 accordance with the oxidation stages C3/4 and R2-4 given by Haggerty (1991). Additionally,
233 shrinkage cracks and a mottled texture of the grains point to some degree of maghemitization
234 of titanomagnetite (Fig. 4c). The sulfide phases are of secondary origin, because they are
235 often found along cracks and veins and are associated with carbonate and quartz (Fig. 4d).
236 Some pyrite grains are altered and replaced by magnetite (Fig. 4d) suggesting a change in
237 fluid chemistry or physico-chemical conditions. Therefore, magnetite is not only produced by
238 oxy-exsolution of titanomagnetite or breakdown of olivine but also by secondary growth. This
239 magnetite shows a net-like porous texture and small, 8 – 20 μm sized euhedral cubes (Fig.
240 4d). Fig. 4e shows the growth of such secondary magnetite along a $\sim 20 \mu\text{m}$ wide vein. The
241 marked area in Fig. 4e is shown with higher magnification in Fig. 4f. On the left side of the
242 photograph, areas possibly representing ilmenite-lamellae can be observed. These areas seem
243 to be relics of exsolved titanomagnetite, where both, titanomagnetite and ilmenohematite have
244 been dissolved. The alteration products consisting of dark grey areas with needle-like crystals
245 are too small to be reliably analyzed, but the data are very similar to an ilmenite composition
246 with up to 9.4 wt.% MnO. For comparison, the homogeneous ilmenohematites have MnO
247 contents of 1.62 – 2.32 wt.%. In some cases the ilmenite-lamellae in titanomagnetite are
248 dissolved and partly replaced by titanite leaving behind a “ghost” texture (Fig. 4b). Also some
249 titanomagnetite is dissolved, which probably supplied the material for the growth of
250 secondary magnetite (Fig. 4d – f; see also discussion). These microscopic observations imply
251 that the secondary magnetite must be considered for the interpretation of the high NRM
252 intensity and χ -values.

253 For the strongly magnetic lower part of the Stardalur profile two groups of oxide textures can
254 be distinguished. Group 1 (Fig. 5a and b) is characterized by rather dendritic and cruciform
255 titanomagnetite with small grain sizes of 5 – 10 μm (max. 20 μm in length). These grains
256 show exsolution textures typical for high temperature oxidation and shrinkage cracks
257 indicating maghemitization. The high opaque mineral content of up to 15 vol.% is reflected in

258 the highest values for NRM intensity and χ (see also Fig. 3). This texture is characteristic for
259 rapid cooling as observed in submarine basalts or marginal parts of subaerial lava flows (e.g.
260 Kontny et al., 2003). Vesicles of up to 1 mm are filled with predominantly chlorite, associated
261 with pyroxene + quartz \pm magnetite and carbonate + titanite, respectively. Whereas no
262 ilmenohematite was found in this group, the second group clearly contains ilmenohematite
263 (Fig. 5c). The ilmenohematite grain sizes range between 12 and 80 μm with partly elongated
264 skeletal shapes. The titanomagnetite shows a dense network of ilmenite-lamellae, and
265 shrinkage cracks (Fig. 5c and d). This second group shows a distinct bimodal grain size
266 population ranging from dendritic, cruciform to xenomorphic grains in the groundmass with
267 less than 10 μm size to subhedral and euhedral grains with 20 – 80 μm in size (Fig. 5d).

268 In contrast to the strongly magnetic lower part of the profile the upper part at the top (around
269 ST36.1) with very low magnetic susceptibilities (Fig. 2) consists of a greenish to pale-grey,
270 soft, tuffaceous rock. Below this tuffaceous rock a zone (~ 4 m thick) of dark greenish to grey
271 rocks with clasts less than 4 mm in size follows with low to intermediate χ -values ($4 - 20 * 10^{-3}$ SI).
272 Microscopic observations revealed altered, rounded glass shards (palagonite) of up to
273 1 mm in size surrounded by carbonate and quartz. The boundaries of the glass shards are lined
274 with abundant opaque phases of up to 20 – 30 μm size, but mostly $< 10 \mu\text{m}$, with irregular
275 shape. With respect to the χ -values, these are most likely titanomagnetite with very low to no
276 Ti content. The ferrofluid is attracted to almost all opaque phases in this rock. Additionally
277 some sulfide phases (up to 40 μm) occur, of which some are found in titanomagnetite and
278 therefore, could have crystallized first and acted as nuclei for the Fe-Ti oxide.

279

280 *3.2 Alternating field and thermal demagnetization*

281 Alternating field (AF) at room temperature and in air atmosphere and thermal
282 demagnetization experiments in air atmosphere were done to get information about the
283 stability of remanence and the kind of mineral(s) carrying the remanence. Generally, the
284 median destructive field (MDF, the field that is necessary to remove half of the NRM) of the
285 Stardalur basalts ranges between 13 and 34 mT (Table 1). In comparison with AF
286 demagnetization experiments done on crushed annealed magnetite (with TRM,
287 thermoremanent magnetization, of 0.1 mT, Dunlop et al., 2004), the Stardalur rocks show
288 similar demagnetization behavior like the samples in the pseudo-single-domain to multi-
289 domain size range (compare Fig. 6a in this publication with Figs. 2, 5 in Dunlop et al., 2004).
290 According to microscopic observations (see above) and temperature dependent susceptibility

291 measurements (see below, Fig. 8) two groups of magnetic behavior have been distinguished,
292 which will be described in the following using representative samples ST101.0 and ST135.15.
293 Fig. 6 presents AF and thermal demagnetization curves for these two samples.

294 Stepwise AF demagnetization (Fig. 6a) shows a continuous decrease of magnetization with
295 increasing magnetic field amplitude, but the derived MDF is significantly higher in sample
296 ST135.15. In regard to the oxide textures of the samples (ST101.0 shows much smaller grain
297 sizes than ST135.15) this result may be surprising. But the large oxidized titanomagnetite
298 grains in ST135.15 contain many ilmenite-lamellae developed during high temperature
299 oxidation subdividing the originally homogeneous titanomagnetite grains. This type of texture
300 can cause MDF values in the range around 30 – 40 mT, as described e.g. for oxidized
301 subaerial basaltic lava of Hawaii (Kontny et al., 2003).

302 Thermal demagnetization curves for the representative samples (Fig. 6b and c) show almost a
303 constant course of magnetization until 300 °C. After heating to higher temperatures NRM
304 intensity decreases continuously resulting in a blocking temperature (T_B) of ~ 590 °C. A very
305 small portion of the NRM still appears above 600 °C and vanishes at 700 °C (Fig. 6 and Fig.
306 7). A high T_B of more than 590 °C, typical for a maghemite-like phase, can be assumed for
307 some samples studied by Fridleifsson and Kristjansson (1972), who found T_C higher than 590
308 °C using strong-field thermomagnetic measurements. After each demagnetization step, we
309 measured χ to check if chemical changes occurred during heating. For sample ST101.0 a very
310 strong decrease in susceptibility has been observed. Less than 10 % of the initial values
311 remain after the final heating step at 700 °C. This observation clearly indicates, that the
312 magnetic phase, which should be most likely magnetite according to its T_B at 590 °C, is not
313 stable during heating. Based on own unpublished measurement of synthetic and natural
314 magnetite, this is unusual for pure stoichiometric magnetite, and therefore we assume that the
315 magnetite is cation-deficient and transforms to hematite during heating. While almost 50 % of
316 the NRM is lost already at 480 °C for ST101.0, thermal demagnetization of ST135.15
317 revealed a different behavior with a stronger temperature resistance. Indeed the blocking
318 temperatures are the same but 50 % of the NRM is retained until 560 °C. Above that
319 temperature, a steep decrease can be observed. Furthermore, less alteration during heating is
320 indicated by the susceptibility, which is 2/3 that of the initial value after heating to 700 °C.
321 While sample ST101.0 shows a change in color from grey to deep red, in sample ST135.15
322 only some areas have changed to red color after heating above 600 °C. These observations are
323 corroborated by the Mössbauer findings, which show less alteration of the ST135.15 sample.
324 At least three explanations are conceivable up to now for this difference: 1) ST101.0 exhibits

325 a stronger degree of cation-deficiency resulting in stronger thermal instability, 2) ST135.15 is
326 less sensitive to maghemitization because some parts of the oxidized titanomagnetite grains
327 resist oxidation due to the large grain size, and 3) ST101.0 contains more magnetite derived
328 from oxidation of olivine, this magnetite has lower MDF and less thermal stability than
329 magnetite derived from exsolution of titanomagnetite. Further experiments have been
330 conducted to unravel these questions.

331

332 *3.3 IRM acquisition and thermal demagnetization of three-component IRM*

333 The acquisition of isothermal remanent magnetization (IRM) up to 1.25 T at ambient
334 temperature gave similar results as the AF demagnetization curves. For ST135.15 higher field
335 amplitudes are needed to impress a magnetization: ST101.0 is saturated already at 200 mT,
336 while a magnetic field of at least 400 mT is needed for ST135.15 (Fig. 7a). This is again a
337 factor of two as already observed for the MDF values. Despite the difference in NRM
338 intensity, the saturation remanence is nearly the same for both samples.

339 Thermal demagnetization of three-component IRM is used to identify the influence of
340 different coercive minerals on the magnetization (Lowrie, 1990). In this experiment, the
341 maximum field of 1.25 T is applied parallel to the z-axis of the sample cylinder, then 500 mT
342 along the y-axis and the lowest field of 200 mT in direction of the x-axis. Subsequent thermal
343 demagnetization of IRM with respect to the axis of applied field is shown in Fig. 7b and c.
344 For both samples a similar behavior can be observed. The initial decrease until 150 °C is
345 attributed to some kind of viscous remanent magnetization, which would disappear after some
346 time of relaxation (A. Hirt, pers. comm. 2006). At higher temperatures for both samples a
347 more or less continuous decrease in IRM intensity, typical for multi-domain magnetite, can be
348 observed with T_B of ~ 510 and 615 °C for ST101.0 and 580 and 615 °C for ST135.15,
349 respectively. The IRM is almost entirely carried by the low coercive phase (x-axis, 200 mT)
350 suggesting that there is no contribution of an ilmenohematite phase or another high coercive
351 mineral like e.g. goethite to the remanent magnetization of the Stardalur rocks. Only for
352 ST135.15 a small influence of a higher coercive phase is seen due to higher IRM intensity of
353 y-axis. This observation is in agreement with the IRM acquisition curve (Fig. 7a) and is
354 probably related to the intense exsolution texture of the titanomagnetite grains and/or the
355 occurrence of cation-deficient (titano)magnetite (Özdemir et al., 1993).

356

357 *3.4 Temperature dependent magnetic susceptibility*

358 Temperature dependent magnetic susceptibility (χ -T curves) is a quick and very sensitive
359 method for the identification of magnetic phases. Furthermore, the degree of reversibility of
360 the heating and cooling run allows an estimate of phase changes, which can be interpreted in
361 terms of the stability of the original magnetic phases.

362 Representative χ -T curves for several selected samples are shown in Fig. 8. For the
363 hyaloclastite sample (ST41.3) from the top of the profile a peak in susceptibility at $-159\text{ }^{\circ}\text{C}$ is
364 observed in a first low temperature run (Fig. 8a), which can be related to the Verwey
365 transition of magnetite. Usually, this crystallographic transition from monoclinic to cubic
366 symmetry occurs in the temperature range -163 to $-153\text{ }^{\circ}\text{C}$ (Verwey, 1939). Due to non-
367 stoichiometry or impurities this transition can be successively shifted towards lower
368 temperatures or disappears (Kakol and Honig, 1989; Özdemir et al., 1993; Moskowitz et al.,
369 1998). During heating in argon atmosphere, a drop in susceptibility at about $584\text{ }^{\circ}\text{C}$ indicates
370 the T_C of magnetite, confirming the low temperature interpretation. In the cooling run only
371 slight to moderate irreversibility is observed. The χ -T curves of all other samples in this study
372 are relatively similar. All samples show a Verwey transition with peak temperatures between
373 -160 and $-154\text{ }^{\circ}\text{C}$ indicating small variations in the degree of oxidation of magnetite (in terms
374 of non-stoichiometry). The Curie temperatures are very consistent and range from 580 to 584
375 $^{\circ}\text{C}$. For some samples a Hopkinson peak just below T_C is observed, suggesting small grain
376 sizes (Fig. 8a and c). During heating in argon atmosphere a more or less developed hump at
377 about 120 to $380\text{ }^{\circ}\text{C}$ is observed in these samples.

378 According to χ -T curves, again the two groups of magnetic behavior can be distinguished
379 (Fig. 8b and c). Group 1 (ST101.0) is characterized by a peak at the Verwey transition, one
380 Curie temperature at $583\text{ }^{\circ}\text{C}$ and a very good reversibility of the heating and cooling branch
381 during measurement in an argon atmosphere. A second low temperature measurement shows
382 a slightly higher Verwey transition temperature than the first low temperature measurement
383 (Fig. 8b). Group 2 (ST135.15) also displays the peak at the Verwey transition but the
384 measurement between room temperature and $700\text{ }^{\circ}\text{C}$ shows a second magnetic phase in the
385 heating run with a magnetic transition (or phase transition?) temperature at $340\text{ }^{\circ}\text{C}$. This
386 phase is unstable during the heating experiment and in the cooling run a phase with a
387 magnetic transition temperature at about $140\text{ }^{\circ}\text{C}$ occurs instead. Instability of some magnetic
388 phases during heating is reported in several studies (e.g. Keefer and Shive, 1980; O'Reilly,
389 1983) and the hump from our study can be most likely interpreted as a T_C or inversion of
390 (titano)magnetite. Another possible candidate to explain the unstable phase could be
391 ilmenohematite with intermediate composition. But remanence experiments (see above, Fig.

392 7) exclude the presence of a higher coercive ferrimagnetic phase. Furthermore, electron
393 microprobe analysis of ilmenohematite gave only Ti-rich compositions near ilmenite with T_N
394 well below room temperature.

395 In order to better define the onset of irreversibility, stepwise heating experiments in argon
396 atmosphere (Fig. 8d) were done. We first heated the sample to 100 °C and cooled it, then we
397 heated the same sample to 200 °C and cooled it again. These heating-cooling cycles were
398 repeated up to 700 °C (for clarity only the measurements up to 450 °C are displayed in Fig.
399 8d). According to this experiment the phase with the magnetic transition temperature at 140
400 °C appears first when the sample is heated up to 350 °C (measurement 4). This is clear
401 evidence, that the breakdown of the phase with the T_C of about 340 °C is directly related to
402 the formation of the phase with the T_C at 140 °C. Furthermore, our experiment has shown,
403 that this phase, once formed, is stable during heating. Curie temperatures at about 140 °C are
404 reported for ferrihydroxides, e.g. goethite ($\alpha\text{-FeOOH}$) at 120 °C (Dunlop and Özdemir, 1997)
405 or ferroxihite ($\delta\text{-FeOOH}$) at 177 °C (Murad, 1996). But ferrihydroxides are not stable during
406 heating to 700 °C, e.g. goethite converts to hematite (Dunlop and Özdemir, 1997). Therefore,
407 we assume that this hump is most likely related to an inversion of titanomaghemite to
408 titanomagnetite of intermediate composition due to annealing and reduction reaction in argon
409 atmosphere.

410 Stoichiometric synthetic and natural magnetite shows a very good reversibility of the heating
411 and cooling curve in an argon atmosphere as well as in air flow (own unpublished data).
412 Therefore we measured our representative Stardalur basalts additionally in air flow (Fig. 9a
413 and b) to better understand the irreversibility of our samples and its implication. During the
414 measurement in an air flow, both samples show a more or less developed hump with T_C at
415 about 400 °C, which is most likely attributed to titanomaghemite, that has been observed
416 already in the argon measurement of ST135.15 (Fig. 8c). A second, very high $T_{C/N}$ at 632 and
417 648 °C, respectively, is probably related to an ilmenohematite with very low Ti content. This
418 ilmenohematite is partly produced by the conversion of instable titanomaghemite during
419 heating. Additionally, for ST135.15 a further T_C at 591 °C occurs, which is not seen in the χ -
420 T curve of ST101.0. This third transition temperature is related to relics of the cation-deficient
421 magnetite, which also converts to Ti-poor ilmenohematite due to oxidation during heating in
422 air. This interpretation is in agreement with the strong irreversibility of the cooling run for
423 both samples, which shows much lower susceptibilities. These low susceptibilities are in
424 accordance with the formation of a mineral with much lower χ -values as e.g. Ti-poor
425 ilmenohematite. According to Hunt et al. (1995 and references therein) magnetic

426 susceptibility of hematite is 20 times smaller than that of magnetite/maghemite. A very small
427 contribution of magnetite/cation-deficient magnetite to the cooling curve is still verified by
428 the second low temperature measurement, which displays only a very weakly developed
429 Verwey transition (see inset with large magnification in Fig. 9a and b). These results indicate
430 that Ti-poor ilmenohematite is produced during heating as a result of titanomaghemite
431 conversion (see e.g. Dunlop and Özdemir, 1997) and oxidation of cation-deficient magnetite,
432 respectively.

433 Repeated heating to 700 °C in air atmosphere proved the stability of the once formed Ti-poor
434 ilmenohematite (Fig. 9c). While the Néel temperature does not change, the amplitude of
435 magnetic susceptibility decreases due to progressive oxidation resulting in further
436 irreversibility. Fig. 9d shows stepwise multiple heating experiments up to 700 °C (with
437 increasing maximum temperature) to find the temperature at which the formation of
438 ilmenohematite starts. The first three heating steps up to 300 °C reveal increasing
439 susceptibilities similar to the single measurement up to 700 °C (Fig. 9b). This behavior is
440 probably related to stress relaxation and/or unpinning of domain walls of the titanomaghemite
441 with a T_C at about 400 °C during heating (Özdemir and Dunlop, 1997). Irreversibility with
442 lower susceptibilities of the cooling branch starts after heating to 350 °C suggesting
443 successive conversion of titanomaghemite to ilmenohematite as well as instability of cation-
444 deficient magnetite. In the 550 °C step, only a slight increase in susceptibility during heating
445 occurs, indicating that the phase with the T_C at about 400 °C is almost completely
446 transformed. While increasing the maximum temperature, each step results in a similar degree
447 of irreversibility. The occurrence of three phases with $T_{C/N}$ between about 550 and 640 °C
448 appear first in the cooling run back from 650 °C. These phases are stable during further
449 heating experiments. The third phase with $T_{C/N}$ of about 550 °C is only observed for
450 ST135.15, while the phase with $T_{C/N}$ of about 590 °C is only weakly developed for ST101.0.

451 Our observations from χ -T curves suggest that the magnetic properties of the Stardalur basalts
452 are mainly related to slightly cation-deficient magnetite and different amounts of
453 titanomaghemite. This interpretation is corroborated from the heating and cooling behavior in
454 argon atmosphere and air flow, and the lower Verwey transition temperature compared to
455 stoichiometric magnetite during the first cooling run. In a second cooling run, the peak at the
456 Verwey transition is shifted 6 - 9 °C to higher temperatures after heating in an argon
457 atmosphere. The maximum transition temperature reported for pure stoichiometric single-
458 crystal magnetite is -149 °C, whereas cation-deficiency or impurities depress the transition
459 temperature down to -191 °C (e.g. Aragón et al., 1985a; Özdemir and Dunlop, 1998;

460 Muxworthy and McClelland, 2000). Considering the findings of Aragón et al. (1985b) the
461 shift of the Verwey transition before and after heating is equivalent to a lower degree in
462 cation-deficiency (δ) by 0.002 – 0.003 ($\text{Fe}_{3(1-\delta)}\text{O}_4$). We assume that the annealing process
463 during heating in argon heals cation defects and produces a more stoichiometric magnetite.
464 This conversion from cation-deficient magnetite to more stoichiometric magnetite during
465 heating has not been verified before in earlier studies.

466

467 *3.5 Mössbauer spectroscopy*

468 From the two representative samples ST101.0 and ST135.15 Mössbauer spectroscopy was
469 performed in order to characterize the iron mineralogy and to resolve the changes taking place
470 during heating in argon and air atmosphere. Fig. 10 shows Mössbauer spectra for the fresh
471 and heated materials. The spectra of each sample were analyzed simultaneously, i.e. assuming
472 the presence of the same components in varying amounts. The spectra were analyzed in terms
473 of three sextets and four symmetric quadrupole split doublets.

474 The sextets were assigned to A and B line of magnetite constrained to have the empirical area
475 ratio $B/A = 1.9$ and zero quadrupole shift ($2\mathcal{E} = \Delta E_Q = 0.0$ mm/s) and a ferric oxide. The
476 internal area ratio of sextet lines were 3:2:1:1:2:3. The lines were assumed pair-wise alike (i.e.
477 lines 1 and 6, 2 and 5, 3 and 4 having the same line-width (Γ), respectively). Due to overlap
478 of the inner lines (3 and 4) with paramagnetic components, the constraint $\Gamma_{25} = (\Gamma_{16} + \Gamma_{34})/2$
479 was applied. The doublets were assigned to ilmenite, Fe(II) in pyroxene, unspecified Fe(III)
480 and a Fe(II) having relatively high quadrupole splitting (results are listed in Table 2). The
481 hyperfine parameters of magnetite are found to be in good agreement with the assignment and
482 the slightly reduced field from table values suggesting small level of impurities. The
483 hyperfine field and the quadrupole shift of the ferric oxide denote that this component
484 originates from hematite. The quadrupole splitting of the Fe(II) component is reduced in
485 comparison with olivine, but is consistent with serpentine or a mixture of both. Small misfits
486 in the spectra could suggest a small level of non-stoichiometry of magnetite or the presence of
487 maghemite < 3 % of the spectral area of fresh samples. These results agree largely with
488 Helgason et al. (1990), who found pure and homogeneous magnetite as the magnetically
489 relevant mineral. But according to the χ -T curves presented above (Fig. 8 and 9) it is likely,
490 especially in respect to the shift in Verwey transition temperature and the strong
491 irreversibility, that the magnetite is slightly non-stoichiometric. Indeed, the Mössbauer
492 spectrum can be interpreted in terms of non-stoichiometry up to $\delta \approx 0.01$, which corresponds

493 to a shift of the Verwey transition by 30 °C, which is not the case. The χ -T measurements
494 therefore seem to be more sensitive to non-stoichiometry than Mössbauer spectroscopy.

495 Generally, the difference in Mössbauer spectra between fresh ST101.0 and ST135.15 are at
496 least two-fold: 1) spectra of ST101.0 lack an ilmenite signal, which is consistent with
497 microscopic observations (only very fine-grained exsolved titanomagnetite, according to
498 electron microprobe analysis less than 0.54 wt.% TiO₂), 2) a significantly larger contribution
499 of magnetite to the Mössbauer spectra of ST101.0 as reflected by the higher area percentage
500 (56 comparing to 30) resulting in higher NRM intensity and χ . The spectra of material heated
501 in argon atmosphere show almost no change in comparison to the fresh material, in agreement
502 with the χ -T curves of Fig. 8b and c. But significant differences can be observed for the
503 samples heated in air atmosphere. For ST101.0 a large contribution of ferric oxide (hematite
504 with perhaps a small contribution of maghemite) is found, to which the magnetite has
505 completely altered, whereas a small amount of magnetite (7 %) is remaining for ST135.15.
506 But also for ST135.15, almost all of the (cation-deficient) magnetite is transformed to ferric
507 oxide (hematite) during measurement in air atmosphere. The Fe(II) component bonded to
508 silicates like e.g. chlorite is higher for ST101.0. Furthermore, almost the entire Fe(II) is lost
509 during heating in air, whereas for ST135.15 Fe(II) is still present. This relation suggests a
510 higher amount of thermally unstable minerals like e.g. chlorite for ST101.0 and supports the
511 hypothesis of stronger alteration affecting ST101.0. This excellent correlation between χ -T
512 curves and Mössbauer spectra corroborates that the χ -T measurements can be used as a
513 reliable method for the identification of ferromagnetic iron mineralogy.

514

515 **4. Discussion**

516 The strong magnetic anomaly at the Stardalur volcanic complex, situated about 20 km NE of
517 Reykjavik, is caused by an extraordinary strong remanent magnetization of up to 121 A/m
518 related to a high magnetite content. According to different previous studies, following factors
519 seem to account for the unusually high magnetization of these basalts: 1) small grain size, 2)
520 high temperature oxidized titanomagnetite, resulting in almost pure magnetite, 3) symplectic
521 magnetite from oxidized olivine and 4) higher (local) paleomagnetic field intensity
522 (Fridleifsson and Kristjansson, 1972; Helgason et al., 1990; Gunnlaugsson et al., 2003, 2006).
523 However, these features are not unique for the Stardalur basalts and therefore we will revisit
524 different mechanisms controlling abundance, composition and grain size in relation to
525 geologic processes.

526 According to our rock magnetic and magneto-mineralogical investigations the magnetically
527 relevant mineral in these rocks is mainly cation-deficient magnetite. From microscopic
528 observations and the comparison with e.g. Hawaiian basalts (Kontny et al., 2003; Vahle,
529 2005) we can conclude that multiple processes, related to the geodynamic setting, the
530 emplacement and the cooling history of the basalts, affected the texture and composition of
531 the originally homogeneous titanomagnetite (stage I in Fig. 11) resulting in extraordinarily
532 high NRM intensity and magnetic susceptibility. These processes are discussed in the
533 following chapter.

534

535 *4.1 Magma composition and cooling history*

536 During initial cooling and quenching of the lava, the rock acquires a TRM, which depends on
537 the amount and grain size of titanomagnetite. Amount and grain size in turn depend on the
538 lava composition, degree of undercooling and cooling rate (\pm oxygen fugacity) during lava
539 emplacement. Gee and Kent (1997) derived a relationship between FeO_{tot} as an indicator of
540 magma fractionation of submarine glass and NRM ($\text{NRM [A/m]} = -25.8 + 4.44 * \% \text{FeO}_{\text{tot}}$)
541 for axial lavas from the southern East Pacific Rise. Taking a range of 8.5 – 14.3 wt.% FeO_{tot}
542 for Icelandic basalts from the Reykjanes peninsula (picritic to tholeiitic basalts described in
543 Jakobsson et al., 1978) NRM intensities of 12 – 38 A/m could be acquired according to this
544 relationship. This NRM intensity range fits nicely to own unpublished data of surface basaltic
545 rocks from SW-Reykjanes peninsula: 4 – 32 A/m (reduced to 90 % of the data set to exclude
546 extreme values). On the other side, a correlation of geochemical data (Rhodes and Vollinger,
547 2004; Stolper et al., 2004) and NRM intensities (Vahle, 2005) of subaerial and submarine
548 basalts from the Hawaiian Scientific Drilling Project (HSDP-2) gave no reasonable results. In
549 this geodynamic setting the measured NRM intensities ($< 1 - 13$ A/m, 90 % of the data) are
550 much lower than the calculated values on the base of Gee and Kent's (1997) equation (18 –
551 32 A/m). However, Steinthorsson and Sigvaldason (1971) have found for Stardalur basalts a
552 rather high Fe-content of ~ 12 wt.%. Using this value in Gee and Kent's (1997) equation one
553 gets 43 A/m, which is far below the average of 63 A/m. These observations indicate, that
554 besides total Fe-content of the magma, other factors must also control the remanence
555 intensity.

556 More important for the resulting magnetic mineral assemblage than the total Fe-content is the
557 $\text{Ti}/(\text{Ti}+\text{Fe})$ ratio and the oxygen fugacity of the melt. High $\text{Ti}/(\text{Ti}+\text{Fe})$ ratios at the same
558 oxygen fugacity favor the formation of Ti-rich phases like ilmenohematite, while decreasing

559 Ti/(Ti+Fe) ratios enable a higher amount of titanomagnetite at a fixed oxygen fugacity. This
560 relationship was shown in experimental studies in the Fe-Ti-O system (see e.g. Fig. 2 in
561 Lattard et al., in press) and is especially true for compositions above the NNO buffer. The
562 generally high amount of magnetic titanomagnetite in the Stardalur basalt seems to be in
563 agreement with relatively oxidized conditions of the basalt melt (above the NNO buffer) and
564 low Ti/(Ti+Fe) ratios. Except for one single analysis of a sample from 60 m depth, no
565 geochemical data are available for the Stardalur basalts up to now. But analyses from surface
566 rocks of the Reykjanes peninsula (SW-Iceland) by Jakobsson et al. (1978) revealed
567 compositions lower in titanium (total iron is similar, resulting in lower Ti/(Ti+Fe) ratios) in
568 comparison with data from e.g. HSDP-2 basalts (Rhodes and Vollinger, 2004; Stolper et al.,
569 2004). The single Stardalur analysis has slightly higher total iron and titanium resulting in
570 Ti/(Ti+Fe) ratios intermediate between Reykjanes and Hawaii. Both, the Reykjanes and
571 Hawaiian basalts show in part similar concentrations of magnetic minerals, but the Icelandic
572 rocks exhibit mostly significantly higher NRM intensity and magnetic susceptibility. This
573 feature is related to the lower ilmenohematite contents of the Icelandic basalts, reflecting a
574 magma composition with low Ti/(Ti+Fe) ratio, resulting in higher titanomagnetite abundance
575 relative to ilmenohematite and therefore higher NRM intensity and χ .

576 Investigations on the remanence properties of synthetic Fe-rich basalts (18.9 % FeO_{tot}) from
577 Brachfeld and Hammer (2006) have shown that the acquisition of thermoremanent
578 magnetization is linked to the oxygen fugacity of the melt and the resulting magnetic mineral
579 assemblage. Samples synthesized at the iron-wüstite (IW) buffer have a very low
580 concentration of remanence-carrying grains, samples synthesized at the quartz-fayalite-
581 magnetite (QFM) and nickel-nickel oxide (NNO) buffers contain a slightly higher amount,
582 and samples synthesized at the manganese oxide (MNO) buffer show the highest
583 concentration of magnetic grains, which are up to 100 μm in diameter. The QFM, NNO and
584 MNO samples acquired TRMs up to 40 A/m in a 10 μT field and even 200 A/m in a 50 μT
585 field, with little or no dependence on cooling rate. However such high values have rarely been
586 observed in terrestrial basalts except zero-age pillow basalts from the East Pacific Rise
587 (Carlut and Kent, 2002) and some basalt occurrences on Iceland (e.g. Gunnlaugsson et al.,
588 2006; this study). Moreover, Carlut and Kent (2002) found strong internal NRM variations on
589 a millimeter scale, whereas the remanence increases sharply in the first centimeter from the
590 marginal part to the pillow interior. This pattern is directly related to a different cooling
591 history in the specific parts of the pillow. In the marginal parts almost no crystals appear due
592 to solidification in less than a few seconds (Griffiths and Fink, 1992), whereas the inner part

593 cooled slower (~ 250 °C/h) leading to rapid formation of magnetic minerals of up to ~ 40 μm
594 in size (Zhou et al., 2000). Therefore both, oxygen fugacity and cooling rate must be
595 considered as major parameters affecting the magnetic properties.

596 For the Stardalur basalts two groups have been defined based on the rock magnetic and
597 magneto-mineralogical properties. The texture and grain sizes of group 1 (ST101.0; dendritic
598 to cruciform titanomagnetite, 5 – 20 μm in size) reflect faster cooling in comparison to the
599 group 2 (ST135.15; bimodal spectrum with dendritic to euhedral grains of $< 10 - 80$ μm size).
600 In samples of group 2 a dense network of ilmenite lamellae points to high temperature
601 deuteritic oxidation during slower cooling. The difference in NRM intensity and χ of these two
602 groups is mainly related to the opaque mineral content and its texture, which depends strongly
603 on cooling history as their primary composition should be the same. After their emplacement
604 the Stardalur basalts suffered significant oxidation and alteration. Therefore, we examine
605 more closely the processes during and after cooling as further possible mechanisms for the
606 enhancement of the already high magnetization.

607

608 *4.2 High temperature deuteritic oxidation*

609 Oxide textures of the Stardalur samples imply high temperature deuteritic oxidation during
610 cooling of the lava. This oxidation is typical for subaerial basalts and is responsible for a
611 significant grain size reduction due to multiple sets of Ti-rich ilmenohematite exsolution
612 lamellae (e.g. Fig. 4b) within the originally homogeneous titanomagnetite (see stage II in Fig.
613 11). This oxyexsolution causes a distinct increase of coercivity but not NRM intensity as our
614 studies on basalt drill cores from the HSDP-2 have shown (Kontny et al., 2003; Vahle, 2005).
615 Basalts from the subaerial section of the HSDP-2 drill core with homogeneous
616 titanomagnetite show a T_C of 100 °C ($X_{\text{usp}} \approx 0.70$), while for samples with exsolved
617 titanomagnetite a T_C at 520 °C ($X_{\text{usp}} \approx 0.10$) is observed. Both samples have comparable
618 NRM intensities ranging between 5 – 6 A/m. Therefore, high temperature deuteritic oxidation
619 seems not to be a significant mechanism leading to an increase in NRM intensity but it
620 enhances remanence stability (14 mT and less for samples with homogeneous titanomagnetite
621 and up to 45 mT for exsolved ones).

622 Additionally to the oxidation of Fe-Ti oxides, silicate minerals are altered during this second
623 stage (Fig. 11) forming magnetite, which acquires a stable (T)CRM. Symplectic magnetite (+
624 pyroxene) is produced by the breakdown of olivine through high temperature deuteritic
625 oxidation or reheating (chapter 3.1 and Fig. 4a and 11). This magnetite formation leads to an

626 increase in NRM intensity and χ . The reheating could be induced by later dike intrusions or
627 burial by a new lava flow. Kristjansson (1985) studied the magnetic and thermal effect of dike
628 intrusions (average width of 4 m) into relatively fresh subaerial lava piles in Iceland. The
629 affected area reached less than 0.5 m away from the contact into the lava flows, whereas
630 changes in remanence intensity cannot be clearly resolved due to primary variations. But a
631 change in remanence direction points to a later overprint. On the contrary, Bleil et al. (1982)
632 found abundant secondary magnetite in altered subaerial basalts drilled by the Iceland
633 Research Drilling Project (IRDIP) in E-Iceland. This secondary magnetite, which is interpreted
634 to increase NRM intensity and which changed magnetic polarity, occurs in zones of dense
635 dike intrusions, providing heat for the remagnetization of the lava flows. Furthermore, Hall
636 (1985) reported on samples from the same drilling an increase of χ and magnetization
637 (induced and remanent) towards the dike contacts, which is related to the growth of secondary
638 magnetite leading to a partial to complete remagnetization of the lava flows. According to the
639 lithological descriptions of the Stardalur core, no intrusions have been found, and the
640 discharge of hydrothermal fluids provides not enough heat for the development of symplectic
641 magnetite (> 810 °C, Haggerty and Baker, 1967), leaving reheating by burial beneath younger
642 lava flows as the only other option. Possible reheating is reflected in the recrystallized glass
643 shards of the hyaloclastite sample ST41.3 and the growth of abundant magnetite lining the
644 glass shards. This leads to unusually high NRM intensity and χ (Table 1) of hyaloclastite,
645 which is usually characterized by low values due to strong quenching in water, where only
646 few, small crystals can develop. Therefore, a rather less magnetic behavior (lower
647 magnetization and susceptibility) is expected for those kinds of rocks (see e.g. Kontny et al.,
648 2003; Vahle, 2005).

649 Indeed, Gunnlaugsson et al. (2006) attribute the high magnetization (40 A/m) of some of their
650 Sudurdalur samples (E-Iceland) to the development of symplectic magnetite (by alteration of
651 olivine). Samples with relatively fresh olivine show only 4 A/m, pointing to a strong increase
652 of NRM intensity due to formation of symplectic magnetite. Although, in our Stardalur
653 samples this mechanism seems to be of less importance comparing to the studies of
654 Gunnlaugsson et al. (2006), we found some indications for symplectic magnetite, which
655 locally increases NRM intensity to some extent, especially in regard to the high temperature
656 of remanence acquisition near and above T_C resulting in a TRM (see below for explanation).
657 Therefore, this mechanism seems to be one important factor contributing to the high
658 magnetization values of the Stardalur basalts.

659

660 *4.3 Hydrothermal Alteration*

661 A significant feature of titanomagnetite in the Stardalur samples is the shrinkage cracks (e.g.
662 Fig. 4c, 5c and d), which are a microscopic sign for maghemitization (Petersen and Vali,
663 1987). Generally, maghemitization is described as a low temperature (< 200 – 250 °C)
664 process occurring mainly at the crystal surface or along cracks promoted by an aqueous
665 environment (e.g. Dunlop and Özdemir, 1997). Depending on subaerial or aqueous
666 conditions, the mechanism is oxidation of Fe²⁺ to Fe³⁺ at a crystal surface and diffusion of
667 Fe²⁺ from the crystal interior to a free surface, where the ion is removed and dissolved in
668 water. Oxidation is therefore a slow process, partly controlled by diffusion rates of Fe²⁺ and
669 the distance to the surface. As a result, the oxidized titanomagnetite gets enriched in Fe³⁺. Due
670 to removal of Fe²⁺ charge balancing vacancies are created leading to the generation and
671 increase of internal stresses in the crystal lattice until it breaks.

672 Curie temperatures of maghemite are reported between 470 and 695 °C (Dunlop and
673 Özdemir, 1997, and references therein), but it can seldom be measured because it usually
674 inverts to magnetite or hematite between 250 and > 750 °C. On the contrary, e.g. Helgason et
675 al. (1992) found stable maghemite in olivine basalts from Iceland using Mössbauer
676 spectroscopy. At 600 °C maghemite is stable in an oxidizing environment for several hours,
677 little maghemite is present after heating for 2 hours in an inactive atmosphere, while the
678 maghemite converts to magnetite already after 30 minutes under reducing conditions (see also
679 Gunnlaugsson et al., 2002). The χ -T measurements in argon and air of all other samples point
680 to cation-deficient magnetite converting to (stoichiometric) magnetite and Ti-poor
681 ilmenohematite, respectively (Fig. 8b and b and Fig. 9a and b). The irreversibility, observed
682 during our measurements, is probably related to cation-deficient magnetite, which is less
683 stable during heating, in comparison to a rather stable behavior of fully oxidized maghemite
684 found by e.g. Helgason et al. (1992) and Gunnlaugsson et al. (2002).

685 Maghemite or titanomaghemite has also been reported e.g. by Steinthorsson et al. (1992) and
686 Gunnlaugsson et al. (2002) for different Icelandic basalts. The first group of authors suggests
687 the onset of maghemitization taking place subsequent to hydrothermal alteration during burial
688 and reheating of the lava flows at wet conditions. Gunnlaugsson et al. (2002) observed an
689 increase in titanomaghemite content after heating the samples (mixture of titanomagnetite and
690 titanomaghemite) to 500 – 600 °C at oxidizing conditions. During this experiment,
691 titanomagnetite gets depleted in Ti due to exsolution processes. Additionally, hematite forms
692 when heated to ~ 700 °C. In case of the Stardalur basalts the instability of titanomaghemite

693 and cation-deficient magnetite starts at ~ 350 °C and ~ 400 °C, when heated in argon and air
694 atmosphere respectively (Fig. 8d, 9d). Therefore, their maghemitization must have occurred
695 mainly below ~ 375 °C on a retrograde path during hydrothermal alteration. Hydrothermal
696 activity is indicated by the presence of zeolites, montmorillonite and chlorite occurring in the
697 groundmass and in vesicles (stage IIIa in Fig. 11). Our thermomagnetic measurements
698 suggest, that no cation-deficient (titano)magnetite should have survived in the basalt, if the
699 rocks would have been reheated to > 400 °C after maghemitization.

700 Maghemitization of ocean basalts is suggested to cause a decrease of NRM intensity (e.g.
701 Matzka et al., 2003), which is explained by the lower saturation magnetization of
702 titanomaghemite compared to titanomagnetite (e.g. magnetite: 480 kA/m, maghemite: 380
703 kA/m, Dunlop and Özdemir, 1997). But the development of shrinkage cracks divides the
704 grain into smaller pieces and possibly leads to an increase or at least no change in NRM
705 intensity as far as no magnetostatic interactions occur. Studies of Helgason et al. (1992) and
706 Gunnlaugsson et al. (2002) suggested titanomaghemite as the stable carrier of NRM intensity
707 in Icelandic basalts. Therefore, oxidation of titanomagnetite to titanomaghemite must not
708 necessarily lead to a reduced NRM intensity. For samples from the HSDP-2 even a slight
709 increase of NRM intensity with depth (and age) is observed, despite the occurrence of low
710 temperature oxidized titanomagnetite (Vahle, 2005). Comparing the different temperature
711 stability of ST101.0 and ST135.15 (Fig. 6b and c, Fig. 9a and b) one may expect a stronger
712 degree of maghemitization (and overall alteration) for ST101.0 due to stronger irreversibility
713 during heating in air (see also significantly lower χ after thermal demagnetization to 700 °C).
714 At least three explanations are conceivable up to now for this difference: 1) ST101.0 exhibits
715 a stronger degree of cation-deficiency resulting in stronger thermal instability (due to small
716 grain sizes diffusion has almost totally affected the grains), 2) ST135.15 is less sensitive to
717 maghemitization because some parts of the oxidized titanomagnetite grains resist
718 maghemitization due to the large grain size (slower diffusion, oxidation not uniform but
719 varies with grain diameter), and 3) ST101.0 contains more magnetite derived from oxidation
720 of olivine (this magnetite has less thermal stability than magnetite derived from exsolution of
721 titanomagnetite). If this is true, the stronger “maghemitized” (altered) sample (ST101.0)
722 shows much higher NRM intensity and χ , which opposes studies of e.g. Matzka et al. (2003).
723 Although these higher values are mostly related to other factors like grain size and
724 concentration of magnetic minerals, this relation implies, that in case of the Stardalur basalts
725 maghemitization during stage IIIa hydrothermal alteration did not lead to a significant
726 lowering of NRM intensity.

727 The maghemitization at stage IIIa and the associated shrinkage cracks in the oxidized
728 titanomagnetite crystals served as pathways for hydrothermal fluids, which altered
729 titanomagnetite as well as ilmenohematite along the cracks and at the margins (Fig. 4c) by
730 dissolution. This alteration leads to the formation of titanite \pm chlorite (stage IIIb in Fig. 11),
731 whereas the dissolution and replacement of ilmenite-lamellae in titanomagnetite created
732 “ghost” textures (Fig. 4b). According to Ade-Hall et al. (1971) a minimum temperature of 250
733 °C is necessary for the replacement of ilmenite by titanite. Above 300 °C polycrystalline Ti-
734 hematite occurs pseudomorph after titanomagnetite. As we have rarely observed hematite but
735 titanite in various amounts, the temperature range of stage IIIb hydrothermal alteration was
736 likely between 250 and 300 °C.

737 The dissolution of ilmenohematite (and titanomagnetite) during stage IIIb hydrothermal
738 alteration probably supplied material for the growth of secondary magnetite (Fig. 4d – f),
739 which could also contribute to higher NRM. Hall (1985) found an increasing amount of
740 secondary magnetite partly produced during hydrothermal alteration in the lower section of
741 the IRDP especially where primary magnetite has been dissolved. The secondary magnetite
742 contributes to an increase of χ (depending on the ratio of dissolved/newly grown magnetite).
743 Because of the good correlation between NRM and χ (Fig. 3) the formation of secondary
744 magnetite is assumed to increase also NRM intensity, although this increase is presumably
745 small. The intensity of a thermochemical remanence (CRM) acquired during crystal growth at
746 temperatures well below T_C by this secondary magnetite is significantly lower than that of an
747 initial TRM acquired during cooling from or just below T_C (e.g. Haigh, 1958; Kobayashi,
748 1959). Draeger et al. (2006) found for samples from a Quaternary basaltic dike (S-France)
749 with single-domain titanomagnetite only half the remanence intensity acquired at 400 °C
750 compared to a TRM. Remanence intensity could even be reduced due to intensive
751 replacement of primary titanomagnetite grains. The different extent of increase in NRM
752 intensity and χ is probably reflected in the relatively low values of Q-factor (5 – 32). In sight
753 of the high NRM intensities of 18 – 121 A/m one would expect also high values for the Q-
754 factor, especially when compared to rather fresh, young (< 20 ka) surface samples from the
755 Reykjanes peninsula with NRM intensity range between 4 and 32 A/m and Q-factors between
756 20 and 105 (90 % of the data set, unpublished data). Therefore, it is likely that the growth of
757 these secondary magnetite grains at intermediate to low temperatures (300 – 250 °C) leads to
758 a significant increase in χ (and higher induced magnetization) but only slightly higher NRM.
759 Due to the poor reversibility of χ -T curves in air (Fig. 9) it is likely, that this secondary
760 magnetite also is slightly non-stoichiometric.

761

762 *4.4 Paleomagnetic field intensity*

763 Although paleointensity investigations are beyond the scope of our study, the intensity of the
764 paleomagnetic field is one crucial factor for the intensity of NRM. Therefore, the influence of
765 paleointensity on the NRM of the Stardalur basalts is discussed below.

766 From paleointensity studies it is concluded that the strength of the Earth magnetic field
767 fluctuates over the Earth history (e.g. Gee et al., 1996; Wang et al., 2005). Wang et al. (2005)
768 found an increase of NRM intensity of Cretaceous Atlantic and Pacific MORB with
769 increasing age following a depression at 10 – 30 Ma aged rocks. While the decrease of NRM
770 intensities of maghemitized ocean basalts (e.g. Matzka et al., 2003) is explained by the lower
771 saturation magnetization of titanomaghemite compared to titanomagnetite, Wang et al. (2006)
772 excluded by a statistical approach compositional, petrologic, rock magnetic, or paleomagnetic
773 patterns for the Cretaceous increase in NRM intensity. They suggested that the geomagnetic
774 field intensity must have been significantly higher during the Cretaceous than during the
775 Oligocene and Miocene.

776 Fridleifsson and Kristjansson (1972) suggested a higher field intensity of $93 \pm 6 \mu\text{T}$ for the
777 Stardalur rocks, which is almost twice the current value for SW-Iceland. This is partly
778 supported by Carmichael (1970) and Ade-Hall et al. (1972) who derived 64 – 120 μT on
779 dredged Quaternary ocean basalts from 45 ° N, whereas Smith (1967) found only $34 \pm 3 \mu\text{T}$
780 for the upper Cenozoic. The thermal instability of the magnetic relevant phases in the
781 Stardalur rocks hampers reliable paleointensity studies. TRM experiments in different
782 laboratory fields from 15 to 145 μT applied on pillow basalts of the East Pacific Rise (Carlut
783 and Kent, 2002) revealed an almost perfect linear relationship between TRM intensity and
784 field amplitude. The NRM intensity of the Stardalur basalts could therefore be twice as high if
785 they had cooled in a paleomagnetic field, that had an intensity that was twice that of today.

786 In fact, Meynadier et al. (1995) suggested, that the geomagnetic field occasionally becomes
787 quite strong (1.5 – 2 times the average), for instance when recovering after a reversal. The
788 Stardalur basalts are estimated to be extruded during Olduvai Subchron based on two K-Ar
789 datings of nearby rhyolites at the Stardalur caldera (Kristjansson et al., 1980). The Olduvai
790 Subchron (1.95 – 1.77 Ma, Cande and Kent, 1995) is a normal polarity event during
791 Matuyama Chron (negative polarity). Maybe, during this short time interval between polarity
792 transitions the Earth magnetic field has been stronger. However, this increase in
793 paleointensity during Olduvai Subchron has not been confirmed so far. In contrast, relative

794 paleointensity studies on ODP-sediment cores from different localities (equatorial Pacific and
795 Iceland basin 450 km south off Iceland) revealed almost no change for the Olduvai Subchron
796 compared with earlier and later times (Meynadier et al., 1995; Channell et al., 2002;
797 Yamazaki and Oda, 2005). A reasonable cause of higher field intensity is a local increase due
798 to strongly magnetic underlying rocks, as already suggested by Fridleifsson and Kristjansson
799 (1972). However, such an explanation remains vague.

800

801 **5. Conclusions**

802 The strong magnetic anomaly of the Stardalur volcanic complex in Iceland is caused by an
803 extraordinary high remanent magnetization of up to 121 A/m. Although we still cannot
804 present an unequivocal explanation for these extraordinary high values, our study suggests
805 that high NRM is due to a high primary titanomagnetite content formed from a basaltic melt
806 with high oxygen fugacity and low Ti/(Ti+Fe) ratio, related to the geodynamic setting on
807 Iceland. Additional to magma composition and cooling history, multiple processes affected
808 the texture and composition of the originally homogeneous titanomagnetite resulting in a
809 further increase in NRM intensity and magnetic susceptibility.

810 According to our results, originally homogeneous titanomagnetite and ilmenohematite
811 suffered subsequent high temperature deuteric oxidation and/or oxidation by later reheating
812 from younger lava flows producing exsolution textures and symplectic magnetite. Due to the
813 high temperatures of $\sim 500 - 900$ °C (stage II), especially the symplectic magnetite can
814 acquire a high and stable TRM (due to the small grain sizes) increasing the NRM. Our own
815 data and Gunnlaugsson et al. (2003) showed an unusually large proportion of iron located in
816 magnetite (up to 56 % of the area of the Mössbauer spectra, 5 – 10 % is more usual), which is
817 in accordance with the alteration of Fe-bearing silicates (predominantly olivine) at high
818 temperatures with subsequent formation of magnetite, leading to an increase in NRM
819 intensity and χ . The NRM (17.7 A/m) of the hyaloclastite sample at the top of the strongly
820 magnetic basalt lava flows may give an approximation of this contribution to NRM.

821 During the first stage of hydrothermal alteration (stage IIIa, $T < 375$ °C) cation-deficient
822 (titano)magnetite is produced. This early hydrothermal stage seems not to be crucial for the
823 NRM intensity of the Stardalur basalts (it either seems to decrease nor increase NRM
824 significantly), but during maghemitization shrinkage cracks developed, which served as
825 pathways for later stage hydrothermal fluids (stage IIIb, $T \approx 250 - 300$ °C). These fluids
826 partly dissolved the primary Fe-Ti oxides, leading to the formation of titanite and secondary

827 magnetite (with further subsequent maghemitization), which is assumed to carry only a low
828 remanence, whereas magnetic susceptibility increases significantly contributing to the
829 induced magnetization.

830 Although the newly formed magnetite during this hydrothermal stage is not very important
831 for the NRM intensity, we assume that hydrothermal alteration is the key factor for the
832 formation of cation-deficient magnetite from the already existing magnetic minerals. Cation-
833 deficient magnetite is found to be the main carrier of the magnetic properties of the Stardalur
834 basalts and for the first time, it is suggested to be the magnetically relevant mineral,
835 responsible for the strong magnetic anomaly at Stardalur. Furthermore, for the first time the
836 conversion from cation-deficient to more stoichiometric magnetite during laboratory heating
837 has been observed. During this maghemitization the NRM intensity seems to be unchanged.
838 The results of this study can be helpful in explaining other strong magnetic anomalies in
839 basaltic environment on Earth and Mars.

840

841 **Acknowledgements**

842 First we want to thank our Icelandic colleagues from the Iceland GeoSurvey ISOR (G.O.
843 Fridleifsson, A. Gudmundsson, A. Blischke, B. Gautason, H. Franzson) and from the
844 Technical University of Iceland (H. Audunsson) for their excellent support and information
845 exchange during our stay at Iceland in July 2005. Ann Hirt is acknowledged for her help and
846 comments concerning the IRM and thermal demagnetization measurements at ETH, Zurich.
847 The German Research Foundation is acknowledged for funding this work (No. KO1514/3).

848

849 **References**

- 850 Acuña, M.H., Connerney, J.E.P., Ness, N.F., Lin, R.P., Michell, D., Carlson, C.W.,
851 McFadden, J., Anderson, K.A., Reme, H., Mazelle, C., Vignes, D., Wasilewski, P., and
852 Cloutier, P., 1999. Global distribution of crustal magnetization discovered by the Mars
853 Global Surveyor MAG/ER experiment. *Science*, 284: 5415-27.
- 854 Ade-Hall, J.M., Palmer, H.C., and Hubbard, T.P., 1971. The magnetic and opaque
855 petrological response of basalts to regional hydrothermal alteration. *Geophysical Journal*
856 *of the Royal Astronomical Society*, 24: 137-174.
- 857 Ade-Hall, J.M., Ryall, P.J.C., and Gerstein, R.E., 1972. Magnetic results from basalt drill
858 cores from the M.A.R. median valley at 45° N. *Eos Transactions*, 53: 955.

- 859 Aragón, R., Buttrey, D.J., Shepard, J.P., and Honig, J.M., 1985a. Influence of
860 nonstoichiometry on the Verwey transition. *Physical Review B*, 31: 430-436.
- 861 Aragón, R., Shepard, J.P., Koenitzer, J.W., Buttrey, D.J., Rasmussen, R.J., and Honig, J.M.,
862 1985b. Influence of nonstoichiometry on the Verwey transition in $\text{Fe}_{3(1-\delta)}\text{O}_4$. *Journal of*
863 *Applied Physics*, 57: 3221-3222.
- 864 Baker, I., and Haggerty, S.E., 1967. The alteration of olivine in basaltic and associated lavas,
865 part II: intermediate and low temperature alteration. *Contributions to Mineralogy and*
866 *Petrology*, 16: 258-273.
- 867 Bleil, U., Hall, J.M., Johnson, H.P., Levi, S., and Schönharting, G., 1982. The natural
868 magnetization of a 3-kilometer section of Icelandic crust. *Journal of Geophysical*
869 *Research*, 87: 6569-6589.
- 870 Brachfeld, S.A., and Hammer, J., 2006. Rock magnetic and remanence properties of synthetic
871 Fe-rich basalts: Implications for Mars crustal anomalies. *Earth and Planetary Science*
872 *Letters*, 248: 599-617.
- 873 Cande, S.C., and Kent, D.V., 1995. Revised calibration of the geomagnetic polarity timescale
874 for the late Cretaceous and Cenozoic. *Journal of Geophysical Research*, 100: 6093-6095.
- 875 Carlut, J., and Kent, D.V., 2002. Grain-size-dependent paleointensity results from very recent
876 Mid-Ocean Ridge basalts. *Journal of Geophysical Research*, 107:
877 10.1029/2001JB000439.
- 878 Carmichael, C.M., 1970. The Mid-Atlantic ridge near 45° N. VII. Magnetic properties and
879 mineralogy of dredged samples. *Canadian Journal of Earth Sciences*, 7: 239-256.
- 880 Channell, J.E.T., Mazaud, A., Sullivan, P., Turner, S., and Raymo, M.E., 2002. Geomagnetic
881 excursions and paleointensities in the Matuyama Chron at Ocean Drilling Program Sites
882 983 and 984 (Iceland Basin). *Journal of Geophysical Research*, 107: 2114,
883 2110.1029/2001JB000491.
- 884 Draeger, U., Prévot, M., Poidras, T., and Riisager, J., 2006. Single-domain chemical,
885 thermochemical and thermal remanences in a basaltic rock. *Geophysical Journal*
886 *International*, 166: 12-32.
- 887 Dunlop, D. J., and Özdemir, Ö., 1997. *Rock Magnetism*. Cambridge University Press, 573 pp.

- 888 Dunlop, D.J., Xu, S., and Heider, F., 2004. Alternating field demagnetization, single-domain-
889 like memory, and the Lowrie-Fuller test of multidomain magnetite grains (0.6-356 μm).
890 Journal of Geophysical Research, 109: B07102, doi: 07110.01029/02004JB003006.
- 891 Fridleifsson, I.B., 1973. Petrology and structure of the Esja Quaternary volcanic region, SW-
892 Iceland. D. Phil, University of Oxford, 208 p.
- 893 Fridleifsson, I.B., and Kristjánsson, L., 1972. The Stardalur magnetic anomaly, SW-Iceland.
894 Jökull, 22: 69-78.
- 895 Fridleifsson, I.B., and Tomasson, J., 1972. Jarðhitarannsóknir á Stardalssvaedinu 1969-1971.
896 Mimeographed report, Orkustofnun, Reykjavik, 14 p.
- 897 Gee, J., and Kent, D.V., 1997. Magnetization of axial lavas from the southern East Pacific
898 Rise (14°-23°S): Geochemical controls on magnetic properties. Journal of Geophysical
899 Research, 102: 24873-24886.
- 900 Gee, J., Schneider, D.A, and Kent, D.V., 1996. Marine magnetic anomalies as recorders of
901 geomagnetic intensity variations. Earth and Planetary Science Letters, 144: 327-335.
- 902 Griffiths, R.W., and Fink, J.H., 1992. Solidification and morphology of submarine lavas: a
903 dependence on extrusion rate. Journal of Geophysical Research, 97: 19729-19737.
- 904 Gunnlaugsson, H.P., Weyer, G., and Helgason, Ö., 2002. Titanomaghemite in Icelandic
905 basalt: possible clues for the strongly magnetic phase in Martian soil and dust. Planetary
906 and Space Science, 50: 157-161.
- 907 Gunnlaugsson, H.P., Bendtsen, L.S., Bertelsen, P., Binau, C.S., Gaarsmand, J., Goetz, W.,
908 Helgason, Ö., Kristjánsson, L., Knudsen, J.M., Leer, K., Madsen, M.B., Nørnberg, P.,
909 Steinbórsson, S., and Weyer, G., 2003. Magnetic anomalies in Iceland: implications for
910 the magnetic anomalies on Mars. Sixth International Conference on Mars, Pasadena
911 (abstract no. 3025).
- 912 Gunnlaugsson, H.P., Helgason, Ö., Kristjánsson, L., Nørnberg, P., Rasmussen, H.,
913 Steinthorsson, S., and Weyer, G., 2006. Magnetic properties of olivine basalt: application
914 to Mars. Physics of the Earth and Planetary Interiors, 154: 276-289.
- 915 Haggerty, S.E., 1991: Oxide textures – a mini-atlas. In: D.H. Lindsley (editor). Oxide
916 Minerals: Petrologic and magnetic significance. Mineralogical Society of America,
917 Reviews in Mineralogy, 25: 129-219.

- 918 Haggerty, S. E., and Baker, I., 1967. The alteration of olivine in basaltic and associated lavas,
919 part I: high temperature alteration. *Contributions to Mineralogy and Petrology*, 16: 233-
920 257.
- 921 Haigh, G., 1958. The process of magnetization by chemical change. *Philosophical Magazine*,
922 3: 267-286.
- 923 Hall, J.M., 1985. The Iceland Research Drilling Project crustal section: variation of magnetic
924 properties with depth in Icelandic-type oceanic crust. *Canadian Journal of Earth Sciences*,
925 22: 85-101.
- 926 Helgason, Ö., Steinthorsson, S., Madsen, M.B., and Mørup, S., 1990. On anomalously
927 magnetic basalt lavas from Stardalur, Iceland. *Hyperfine Interactions*, 57: 2209-2214.
- 928 Helgason, Ö., Gunnlaugsson, H.P., Steinthorsson, S., and Mørup, S., 1992. High temperature
929 stability of maghemite in partially oxidized basalt lava. *Hyperfine Interactions*, 70: 981-
930 984.
- 931 Hunt, C.P., Moskowitz, B.M., and Banerjee, S.K., 1995. Magnetic properties of rocks and
932 minerals. In T.J. Ahrens (editor): *AGU Reference Shelf 3 - Rock Physics and Phase
933 Relations, A Handbook of Physical Constants*, pp. 189-204.
- 934 Jakobsson, S.P., Jonsson, J., and Shido, F., 1978. Petrology of the Western Reykjanes
935 Peninsula, Iceland. *Journal of Petrology*, 19: 669-705.
- 936 Jonsson, G., Kristjánsson, L., and Sverrisson, M., 1991. Magnetic surveys of Iceland.
937 *Tectonophysics*, 189: 229-247.
- 938 Kakol, Z., and Honig, J.M., 1989. The variation of Verwey transition temperature with
939 oxygen stoichiometry in magnetite. *Solid State Communications*, 70: 967-969.
- 940 Keefer, C.M., and Shive, P.N., 1980. Titanomaghemites: conditions for oxidation, influence
941 of rhombohedral phases, and temperature of inversion. *Earth and Planetary Science
942 Letters*, 51: 199-205.
- 943 Kletetschka, G., and Kontny, A., 2005. Identification of magnetic minerals by scanning
944 electron microscope and application of ferrofluid. *Studia Geophysica et Geodaetica*, 49:
945 153-162.
- 946 Kobayashi, K., 1959. Chemical remanent magnetization of ferromagnetic minerals and its
947 application to rock magnetism. *Journal of Geomagnetism and Geoelectricity*, 10: 99-117.

- 948 Kontny, A., Vahle, C., and de Wall, H., 2003. Characteristic magnetic behavior of subaerial
949 and submarine lava units from the Hawaiian Scientific Drilling Project (HSDP-2).
950 *Geochemistry Geophysics Geosystems*, 4: doi: 10.1029/2002GC000304.
- 951 Kristjansson, L., 1970. Palaeomagnetism and magnetic surveys in Iceland. *Earth and*
952 *Planetary Science Letters*, 8: 101-108.
- 953 Kristjansson, L., 1985. Magnetic and thermal effects of dike intrusions in Iceland. *Journal of*
954 *Geophysical Research*, 90: 10129-10135.
- 955 Kristjansson, L., Fridleifsson, I.B., and Watkins, N.D., 1980. Stratigraphy and
956 paleomagnetism of the Esja, Eyrafjall and Akrafjall Mountains, SW-Iceland. *Journal of*
957 *Geophysics*, 47: 31-42.
- 958 Lattard, D., Engelmann, R., Kontny, A., and Sauerzapf, U., in press. Curie temperatures of
959 synthetic titanomagnetites in the Fe-Ti-O system: effects of composition, crystal
960 chemistry and thermomagnetic methods. *Journal of Geophysical Research*.
- 961 Lowrie, W., 1990. Identification of ferromagnetic minerals in a rock by coercivity and
962 unblocking temperature properties. *Geophysical Research Letters*, 17: 159-162.
- 963 Matzka, J., Krása, D., Kunzmann, T., Schult, A., and Petersen, N., 2003. Magnetic state of
964 10-40 Ma old ocean basalts and its implications for natural remanent magnetization.
965 *Earth and Planetary Science Letters*, 206: 541-553.
- 966 Meynadier, L., Valet, J.-P., and Shackleton, N.J., 1995. Relative geomagnetic intensity during
967 the last 4 m.y. from the equatorial Pacific. *Proceedings of the Ocean Drilling Program,*
968 *Scientific Results*, 138: 779-795.
- 969 Moskowitz, B.M., Jackson, M., and Kissel, C., 1998. Low-temperature magnetic behavior of
970 titanomagnetites. *Earth and Planetary Science Letters*, 157: 141-149.
- 971 Murad, E., 1996. Magnetic properties of microcrystalline iron (III) oxides and related
972 materials as reflected in their Mössbauer spectra. *Physics and Chemistry of Minerals*, 23:
973 248-262.
- 974 Muxworthy, A.R., and McClelland, E., 2000. Review of the low-temperature magnetic
975 properties of magnetite from a rock magnetic perspective. *Geophysical Journal*
976 *International*, 140: 101-114.

- 977 O'Reilly, W., 1983. The identification of titanomaghemites: model mechanisms for the
978 maghemitization and inversion processes and their magnetic consequences. *Physics of*
979 *the Earth and Planetary Interiors*, 31: 65-76.
- 980 Özdemir, Ö., and Dunlop, D.J., 1997. Effect of crystal defects and internal stresses on the
981 domain structure and magnetic properties of magnetite. *Journal of Geophysical Research*,
982 102: 20211-20224.
- 983 Özdemir, Ö., and Dunlop, D.J., 1998. Single-domain-like behavior in a 3-mm natural single
984 crystal of magnetite. *Journal of Geophysical Research*, 103(B2): 2549-2562.
- 985 Özdemir, Ö., Dunlop, D.J., and Moskowitz, B.M., 1993. The effect of oxidation on the
986 Verwey transition in magnetite. *Geophysical Research Letters*, 20: 1671-1674.
- 987 Petersen, N., and Vali, H., 1987. Observation of shrinkage cracks in ocean floor
988 titanomagnetites. *Physics of the Earth and Planetary Interiors*, 46: 197-205.
- 989 Petrovsky, E., and Kapicka, A., 2005. COMMENTS ON "The use of field dependence of
990 magnetic susceptibility for monitoring variations in titanomagnetite composition - a case
991 study on basanites from the Vogelsberg 1996 drillhole, Germany" by de Wall and Nano,
992 *Studia Geophysica et Geodaetica*, 48, 767-776. *Studia Geophysica et Geodaetica*, 49:
993 255-258.
- 994 Pouchon, J.L., and Pichoir, F., 1984. A new model for quantitative X-ray microanalysis, Part
995 I: Application to the analysis of homogeneous samples. *La Recherche Aérospatiale*, 3:
996 167-192.
- 997 Purucker, M., Ravat, D., Frey, H., Voorhies, C., Sabaka, T., and Acuña, M.H., 2000. An
998 altitude-normalized magnetic map of Mars and its interpretation. *Geophysical Research*
999 *Letters*, 27: 2449-2452.
- 1000 Rhodes, J.M., and Vollinger, M.J., 2004. Composition of basaltic lavas sampled by phase-2 of
1001 the Hawaiian Scientific Drilling Project: Geochemical stratigraphy and magma types.
1002 *Geochemistry Geophysics Geosystems*, 5: Q03G13, doi: 10.1029/2002GC000434.
- 1003 Smith, P.J., 1967. The intensity of the Tertiary geomagnetic field. *Geophysical Journal of the*
1004 *Royal Astronomical Society*, 12: 239-258.
- 1005 Steinthorsson, S., and Sigvaldason, G.E., 1971. *Skýrsla um bergfræðirannsóknir við Stardal.*
1006 *Science Institute, University of Iceland, Report.*

- 1007 Steinthorsson, S., Helgason, Ö., Madsen, M.B., Koch, C.B., Bentzon, M.D., and Morup, S.,
1008 1992. Maghemite in Icelandic basalts. *Mineralogical Magazine*, 56: 185-199.
- 1009 Stolper, E.M., Sherman, S., Garcia, M., Baker, M., and Seaman, C., 2004. Glass in the
1010 submarine section of the HSDP2 drill core, Hilo, Hawaii. *Geochemistry Geophysics*
1011 *Geosystems*, 5: Q07G15, doi: 10.1029/2003GC000553.
- 1012 Vahle, C., 2005. Aufbau und Entwicklung des Vulkans Mauna Kea anhand von
1013 gesteinsmagnetischen und magneto-mineralogischen Untersuchungen an Kernen des
1014 "Hawaii Scientific Drilling Project" (HSDP-2). Inaugural-Dissertation zur Erlangung der
1015 Doktorwürde, Naturwissenschaftlich-Mathematische Gesamtfakultät, Ruprecht-Karls-
1016 Universität Heidelberg, pp. 285.
- 1017 Verwey, E.J.W., 1939. Electronic conduction of magnetite (Fe_3O_4) and its transition point at
1018 low temperatures. *Nature*, 144: 327-328.
- 1019 Wang, D., Van der Voo, R., and Peacor, D.R., 2005. Why is the remanent magnetic intensity
1020 of Cretaceous MORB so much higher than that of mid to late Cenozoic MORB?
1021 *Geosphere*, 1: 138-146.
- 1022 Yamazaki, T., and Oda, H., 2005. A geomagnetic paleointensity stack between 0.8 and 3.0
1023 Ma from equatorial Pacific sediment cores. *Geochemistry Geophysics Geosystems*, 6:
1024 Q11H20, doi: 10.1029/2005BC001001.
- 1025 Zhou, W., Van der Voo, R., Peacor, D.R., and Zhang, Y., 2000. Variable Ti-content and grain
1026 size of titanomagnetite as a function of cooling rate in very young MORB. *Earth and*
1027 *Planetary Science Letters*, 179: 9-20.

1028

1029

1030

1031 **Figure captions**

1032 Fig. 1: a) Location of the Stardalur volcanic complex and present zones of volcanism and
1033 crustal spreading (shaded areas) in Iceland (additionally, the glacier (jökull) outlines are
1034 shown; modified from Jonsson et al., 1991); b) geological map with location of the drill site
1035 (modified from Fridleifsson and Kristjánsson, 1972, lines A-B and C-D refer to cross sections
1036 described therein).

1037

1038 Fig. 2: Susceptibility profile of the Stardalur core and location of samples (b: brecciated
1039 zone). The lithological boundaries are picked from the lithological profile described in
1040 Fridleifsson and Tomasson (1972).

1041

1042 Fig. 3: Magnetic susceptibility (measured at field amplitude of 30 A/m) vs. natural remanent
1043 magnetization (NRM) of all sample cylinders.

1044

1045 Fig. 4: Oxide textures of the Stardalur basalts show the processes affecting the magnetic
1046 minerals (a: reflected light, in oil immersion and coated with ferrofluid, b-f: SEM images
1047 taken in backscatter mode): a) symplectic magnetite around former olivine during high
1048 temperature oxidation; b) ilmenite lamellae in titanomagnetite host (partly with dissolved
1049 ilmenite) during high temperature oxidation; c) maghemitized titanomagnetite with shrinkage
1050 cracks working as pathways for hydrothermal fluids altering the Fe-Ti oxides; d) secondary
1051 pyrite (py) and magnetite (mt), associated with carbonate (ca) and quartz (qz); e) secondary
1052 magnetite crystallized along veins; f) the area marked in e) with higher magnification
1053 showing relics of oxidized titanomagnetite surrounded by net-like, porous secondary
1054 magnetite (tmt: titanomagnetite, ilhm: ilmenohematite, plg: plagioclase, cpx: clinopyroxene,
1055 ox: oxidized).

1056

1057 Fig. 5: Different oxide textures of representative samples for group 1 and 2 (SEM images in
1058 backscatter mode): group 1 (a and b, ST101.0): skeletal to dendritic Fe-Ti oxides of small
1059 grain size comparing to group 2 with a bimodal grain size spectrum with skeletal to euhedral
1060 and dendritic crystals for ST135.15 (c) and ST62.9 (d; tmt: titanomagnetite, ilhm:
1061 ilmenohematite, plg: plagioclase, chl: chlorite, cpx: clinopyroxene, ox: oxidized).

1062

1063 Fig. 6: a) Alternating field demagnetization of ST101.0 and ST135.15 with median
1064 destructive field (MDF); b) and c) thermal demagnetization of NRM with accompanying χ -
1065 measurement for both samples.

1066

1067 Fig. 7: a) Acquisition of isothermal remanent magnetization (IRM) for ST101.0 and ST135.15
1068 (J_{rs} : saturation remanence); b) and c) thermal demagnetization of saturated IRM after the

1069 Lowrie method (Lowrie, 1990): first 1.25 T are applied along the z-axis, then 500 mT parallel
1070 to the y-axis and finally 200 mT in direction of the x-axis to identify contributions of minerals
1071 with different coercivity.

1072

1073 Fig. 8: Examples of temperature dependent susceptibility measurements done in argon (a-c);
1074 d) stepwise heating in argon of ST135.15 to display the temperature intervals at which
1075 irreversibility occur (solid line: heating, dashed line: cooling (also indicated by arrows) and
1076 repeated low temperature measurement, respectively).

1077

1078 Fig. 9: Temperature dependent susceptibility for ST101.0 (a) and ST135.15 (b) done in air
1079 with subsequent re-measurement of the heated material (the inset shows the low temperature
1080 measurement in lower scale); c) multiple heating in air to 700 °C of ST101.0 showing the
1081 successive decrease in susceptibility which results in poor reversibility; d) stepwise heating in
1082 air of ST135.15 to display the temperature intervals at which irreversibility starts (solid line:
1083 heating, dashed line: cooling (also indicated by arrows) and repeated low temperature
1084 measurement, respectively).

1085

1086 Fig. 10: Mössbauer spectra of fresh material and material used for temperature dependent
1087 susceptibility measurements in argon and air of ST101.0 and ST135.15.

1088

1089 Fig. 11: Sketch showing the development of titanomagnetite and ilmenohematite textures
1090 from initial cooling/quenching to the latest stage of alteration; additionally, the change in
1091 strength of the relevant magnetic parameters is given (further description see text).

1092

1093

1094 **Tables**

1095 Table 1: Rock magnetic properties of the Stardalur samples (no average values, data of single
1096 cylinders).

sample	depth [m]	lithology	NRM [A/m]	Q	χ (30 A/m) [10 ⁻³ SI]	MDF [mT]	SIRM [A/m]	opaque mineral content [vol.%]
ST36.1	36.1	tuff	0.6	7.5	2.1	27	-	-
ST41.30	41.3	hyaloclastite	17.7	16.4	25.9	32	883	6
ST47.00	47.0	basalt	42.0	14.8	68.3	23	-	-
ST53.60	53.6	basalt	52.6	10.7	118.0	14	1941	11
ST62.90	62.9	basalt	80.3	20.5	93.9	24	3077	10
ST74.90	74.9	basalt	62.2	19.2	78.0	22	-	-
ST101.00	101.0	basalt	90.5	18.4	118.0	18	2489	15
ST111.45	111.5	basalt	25.6	7.5	81.5	13	-	8
ST117.50	117.5	basalt	48.3	24.8	46.8	25	-	7
ST135.15	135.2	basalt	63.0	26.0	58.3	34	2414	9
ST138.10	138.1	basalt	99.2	30.4	78.5	23	-	-

NRM: natural remanent magnetization, Q: Kšnigsberger ratio (for calculation a field intensity of 41.6 A/m was used), χ (30 A/m): magnetic susceptibility measured at 30 A/m, MDF: median destructive field, SIRM: saturation isothermal remanence at 1.25 T

1097

1098

1099 Table 2: Hyperfine parameters obtained from simultaneous analysis of the spectra of ST101.0
1100 and ST135.15 samples. The numbers in the parentheses represent 1 σ error in the last digit.

1101 Quadrupole shift of sextet components is given as 2 ϵ .

ST101.0	magnetite_ A	magnetite_ B	ferric oxide	Fe(II)	Fe(II) pyroxene	Fe(III)	ilmenite
B_{hf} (T)	48.93(5)	45.69(4)	51.45(4)				
δ (mm/s)	0.288(6)	0.666(4)	0.375(5)	1.146(6)	1.12(1)	0.37(2)	1.02(2)
ΔE_Q (mm/s)	0	0	-0.17(1)	2.66(2)	1.99(4)	1.14(2)	0.7(2)
Γ_{16} (mm/s)	0.36(2)	0.45(2)	0.36(2)	0.36(3)	0.51(4)	0.61(3)	0.3(3)
Γ_{34} (mm/s)	0.34(4)	0.30(2)	0.26(2)				
A_fresh (%)		56(3)	1.6(9)	17(2)	10(2)	13(2)	0.8(9)
A_Ar (%)		58(2)	0.5(7)	11(2)	16(2)	12.5(9)	0.8(8)
A_air (%)		3(2)	55(3)	0.3(10)	3(2)	36(3)	0.3(10)

ST135.15	magnetite_ A	magnetite_ B	ferric oxide	Fe(II)	Fe(II) pyroxene	Fe(III)	ilmenite
B_{hf} (T)	48.8(1)	45.61(8)	51.7(2)				
δ (mm/s)	0.27(2)	0.67(1)	0.38(2)	1.13(1)	1.139(4)	0.44(1)	1.03(1)
ΔE_Q (mm/s)	0	0	-0.18(3)	2.66(1)	1.969(3)	0.93(3)	0.71(3)
Γ_{16} (mm/s)	0.37(3)	0.54(4)	0.47(2)	0.32(2)	0.451(5)	0.57(4)	0.32(4)
Γ_{34} (mm/s)	0.28(6)	0.30(3)	0.32(2)				
A_fresh (%)		30(2)	0(2)	12.8(5)	38.0(9)	13(1)	5.1(3)
A_Ar (%)		31(2)	0(2)	8.1(3)	39.6(9)	15.2(4)	5.9(8)
A_air (%)		7(2)	25(2)	6.0(8)	32(2)	22(2)	5.5(2)

1102

1103

Fig. 1

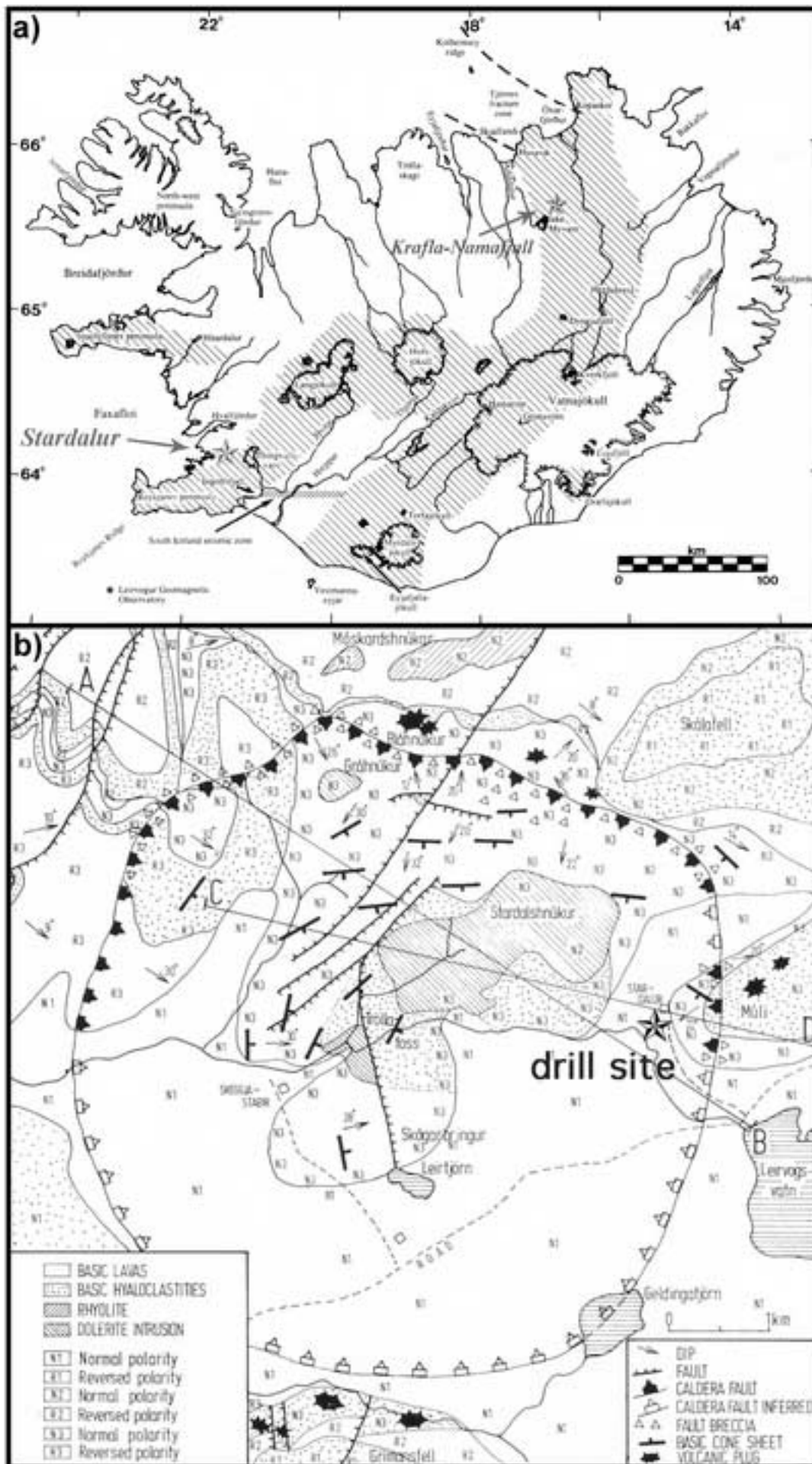


Fig. 2

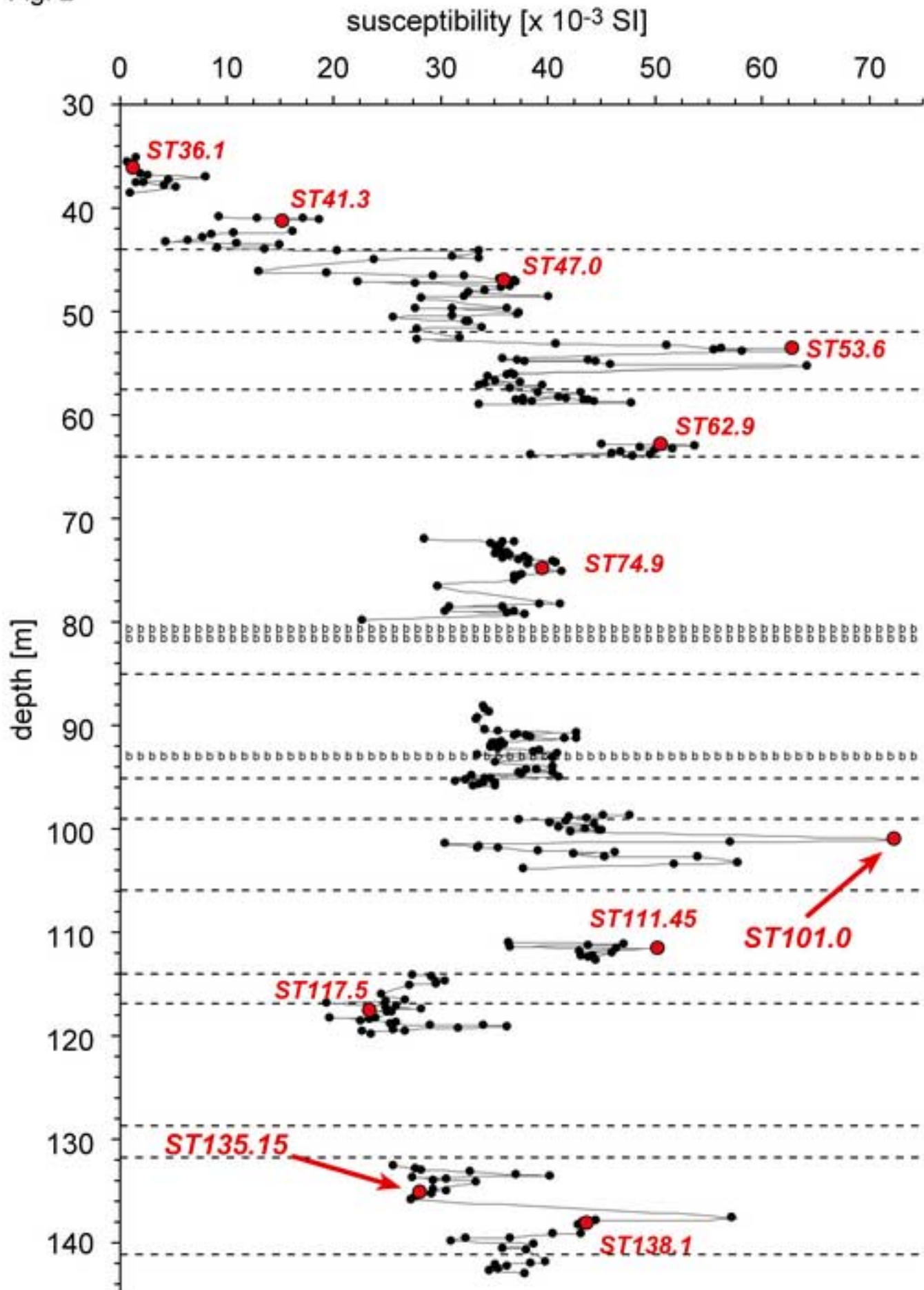


Fig. 3

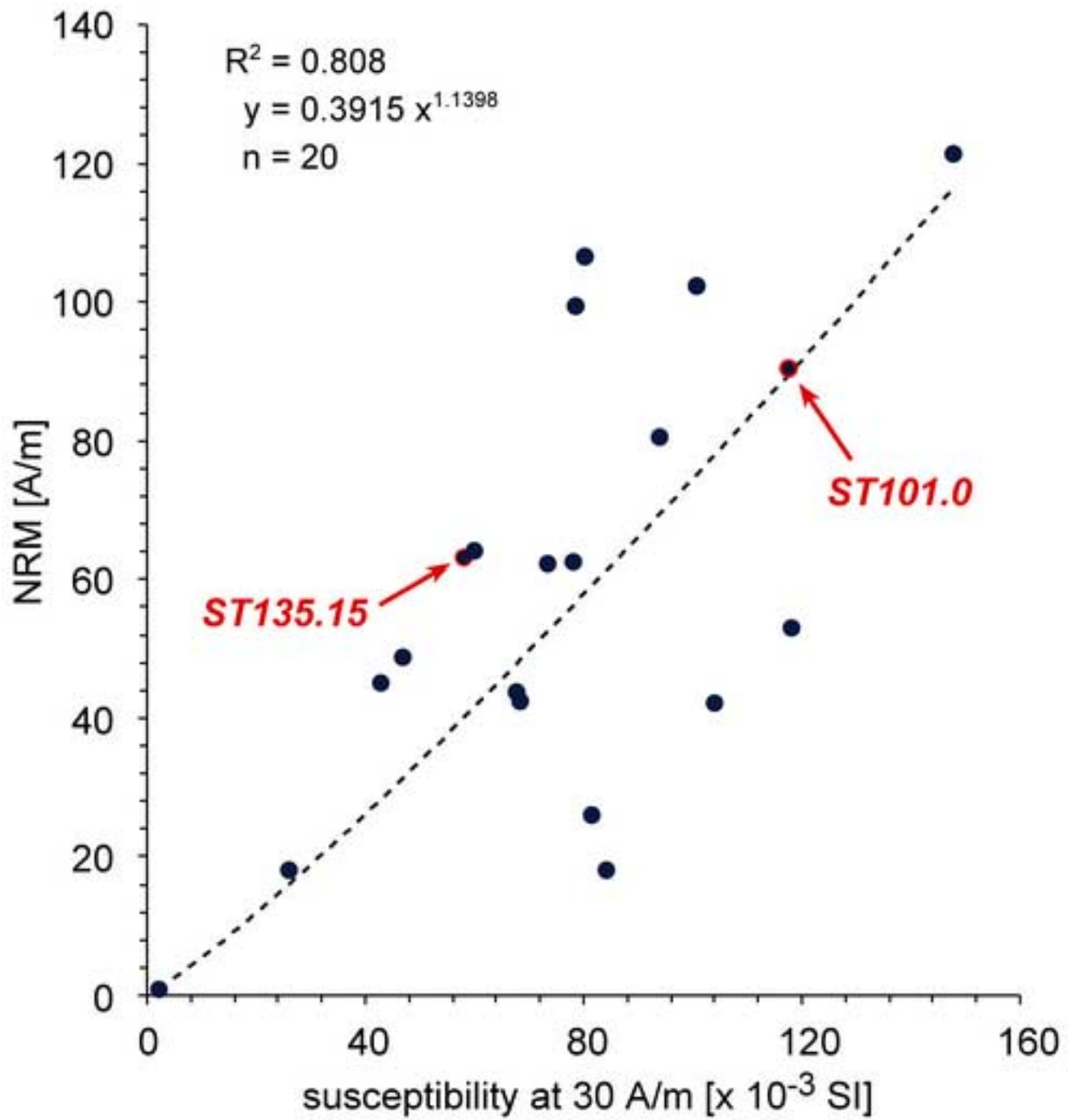


Fig. 4

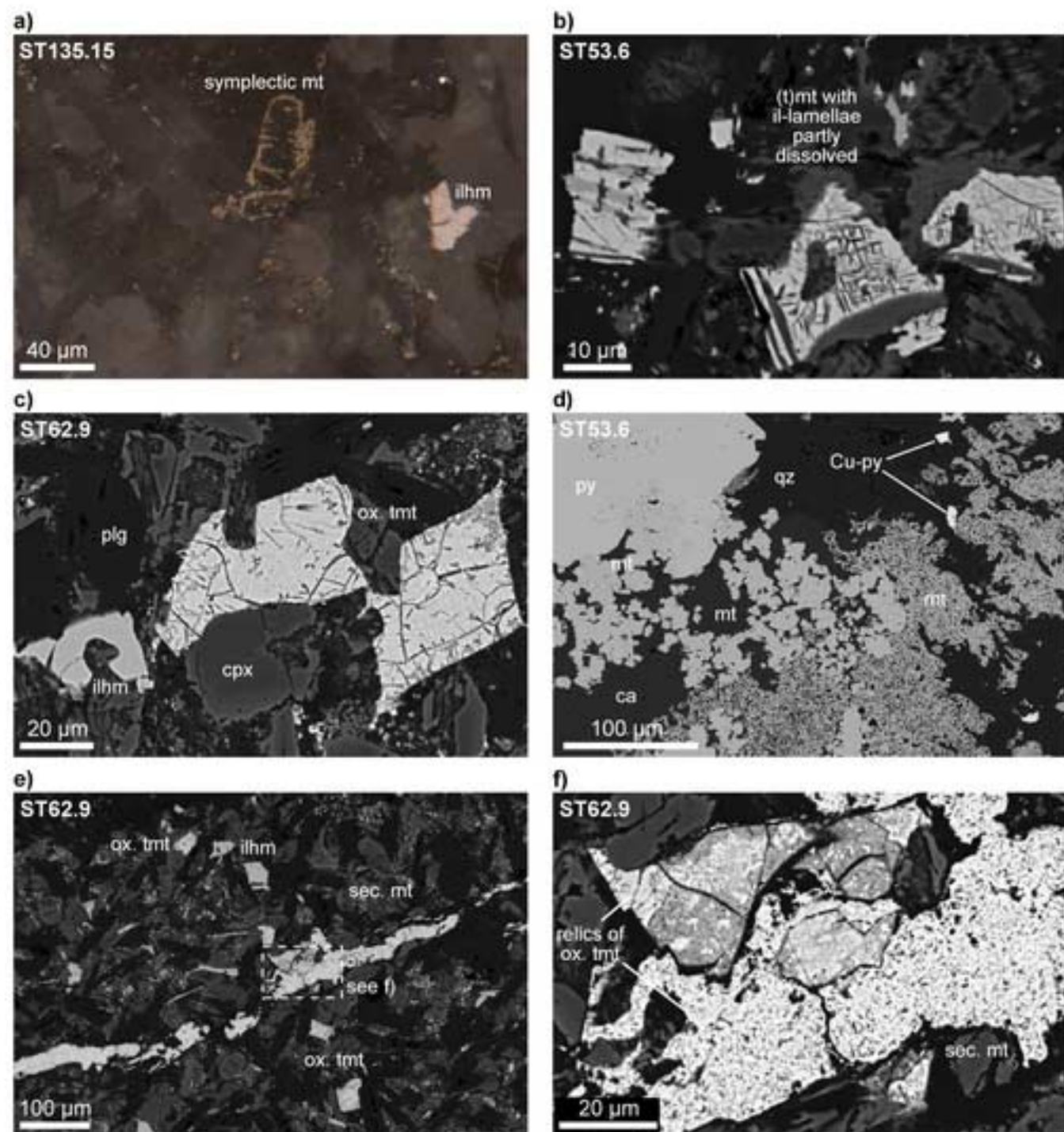


Fig. 5

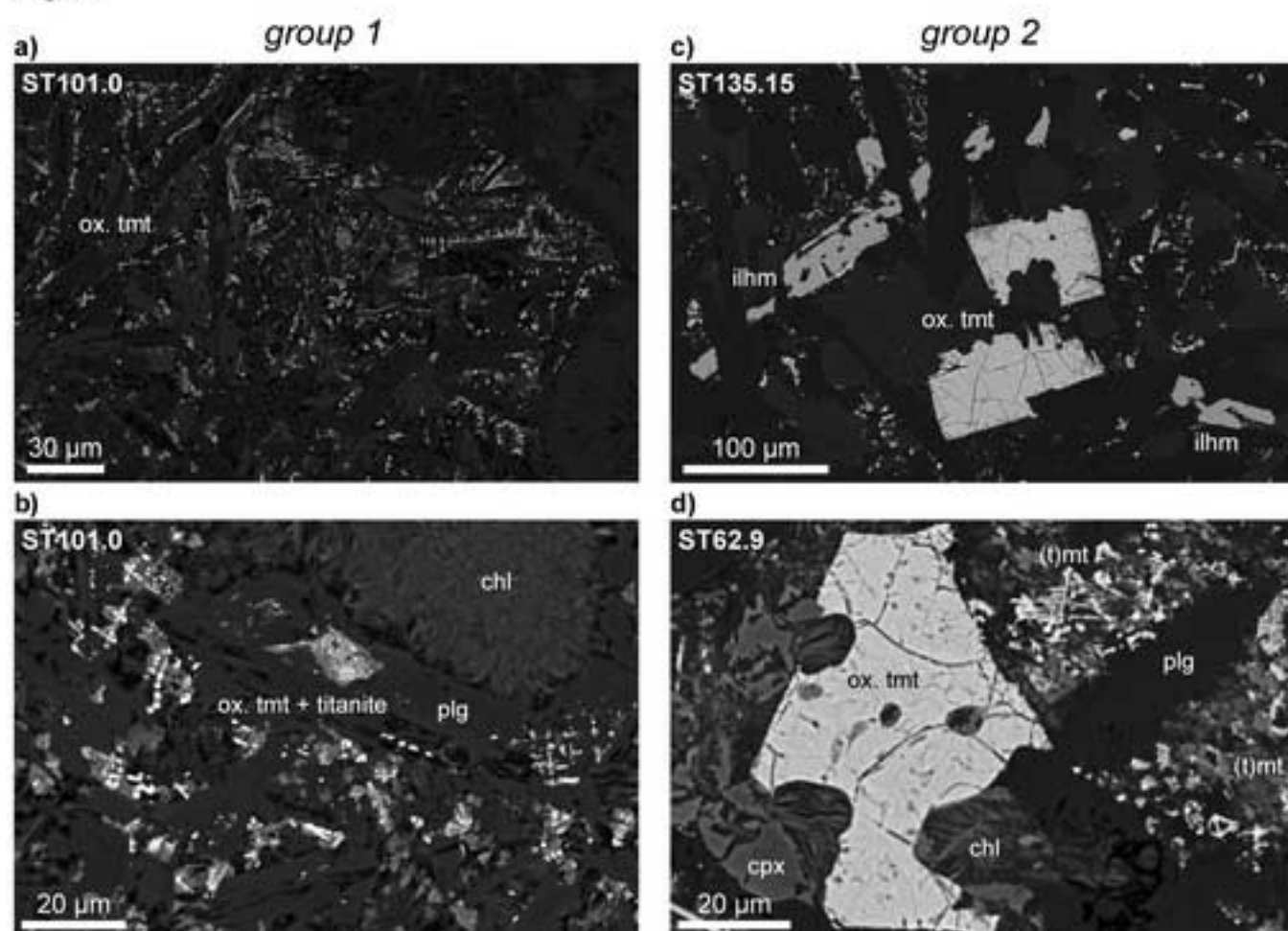


Fig. 6

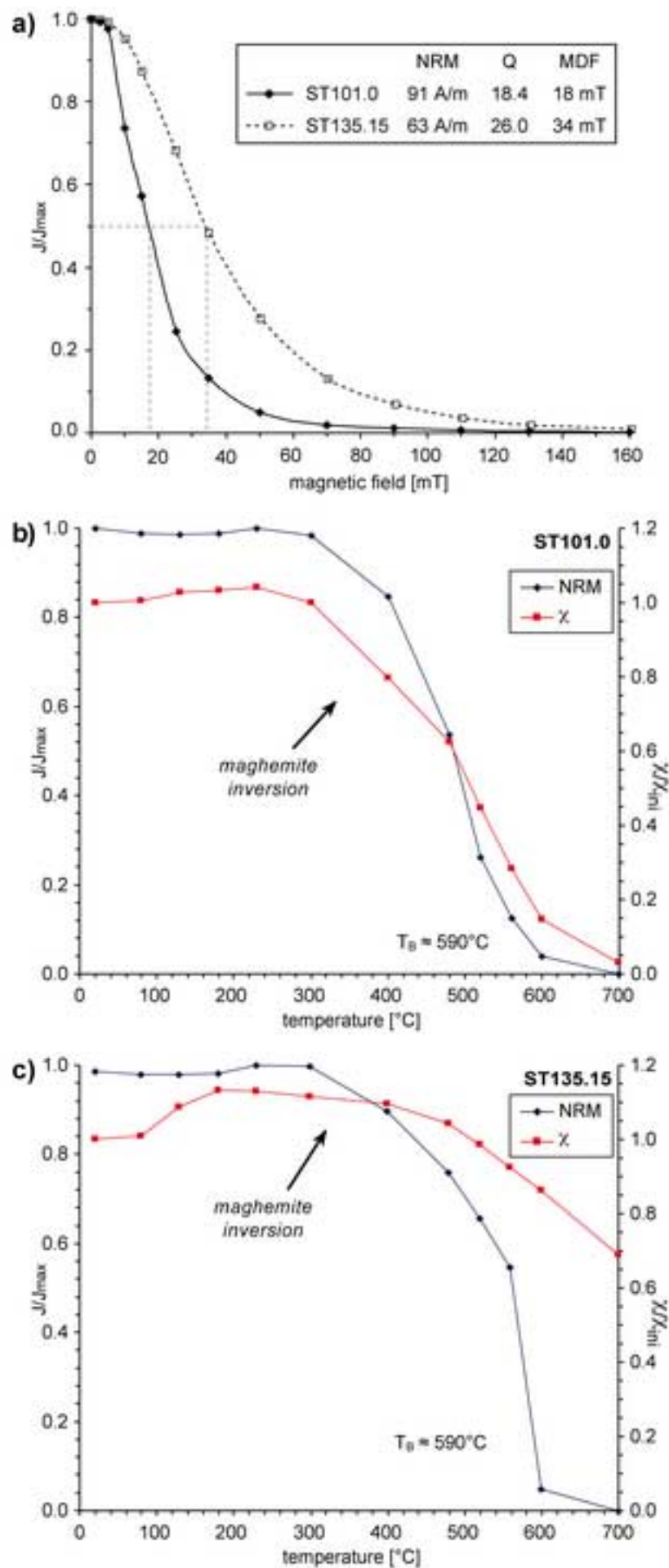


Fig. 7

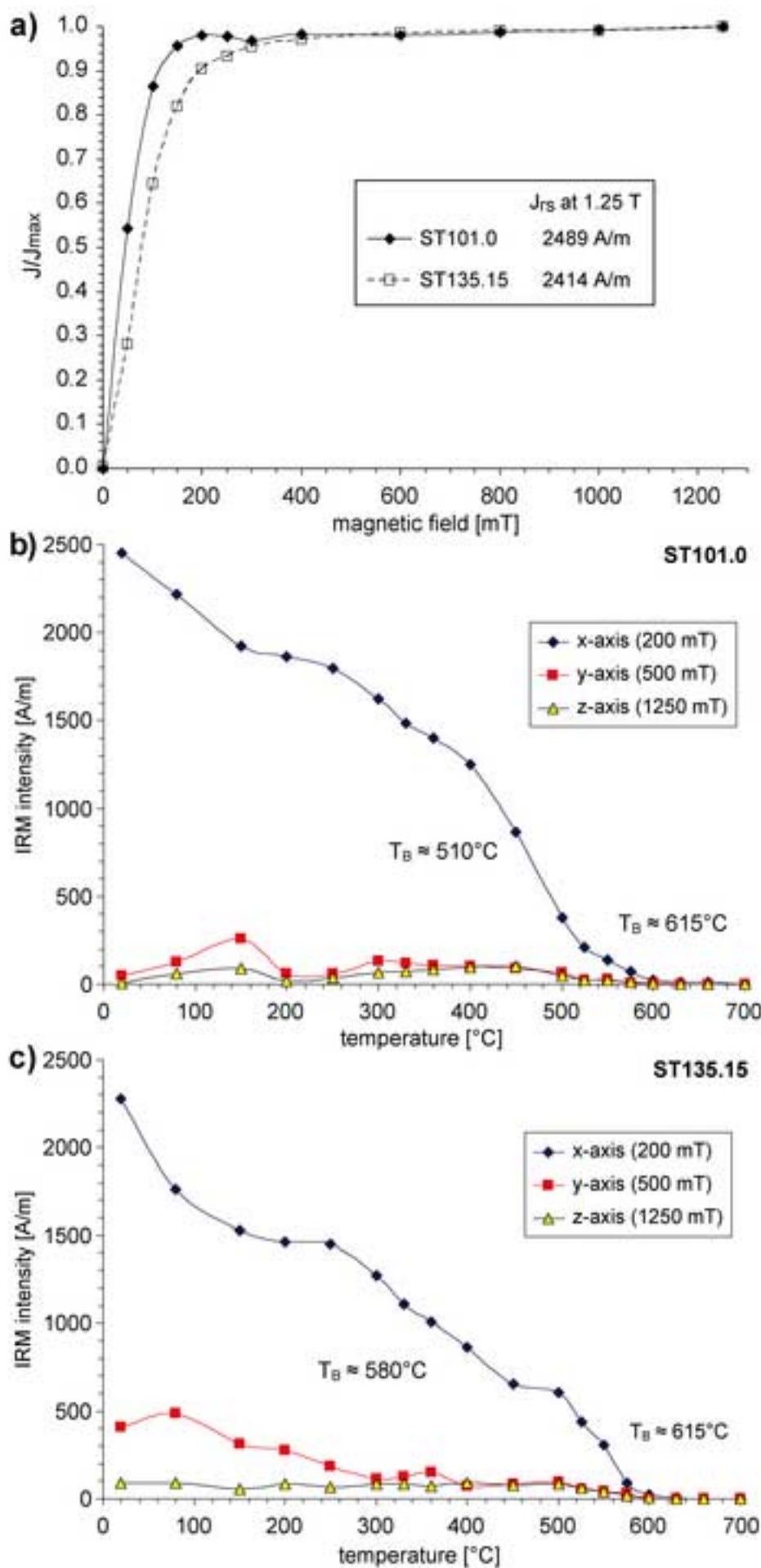


Fig. 8

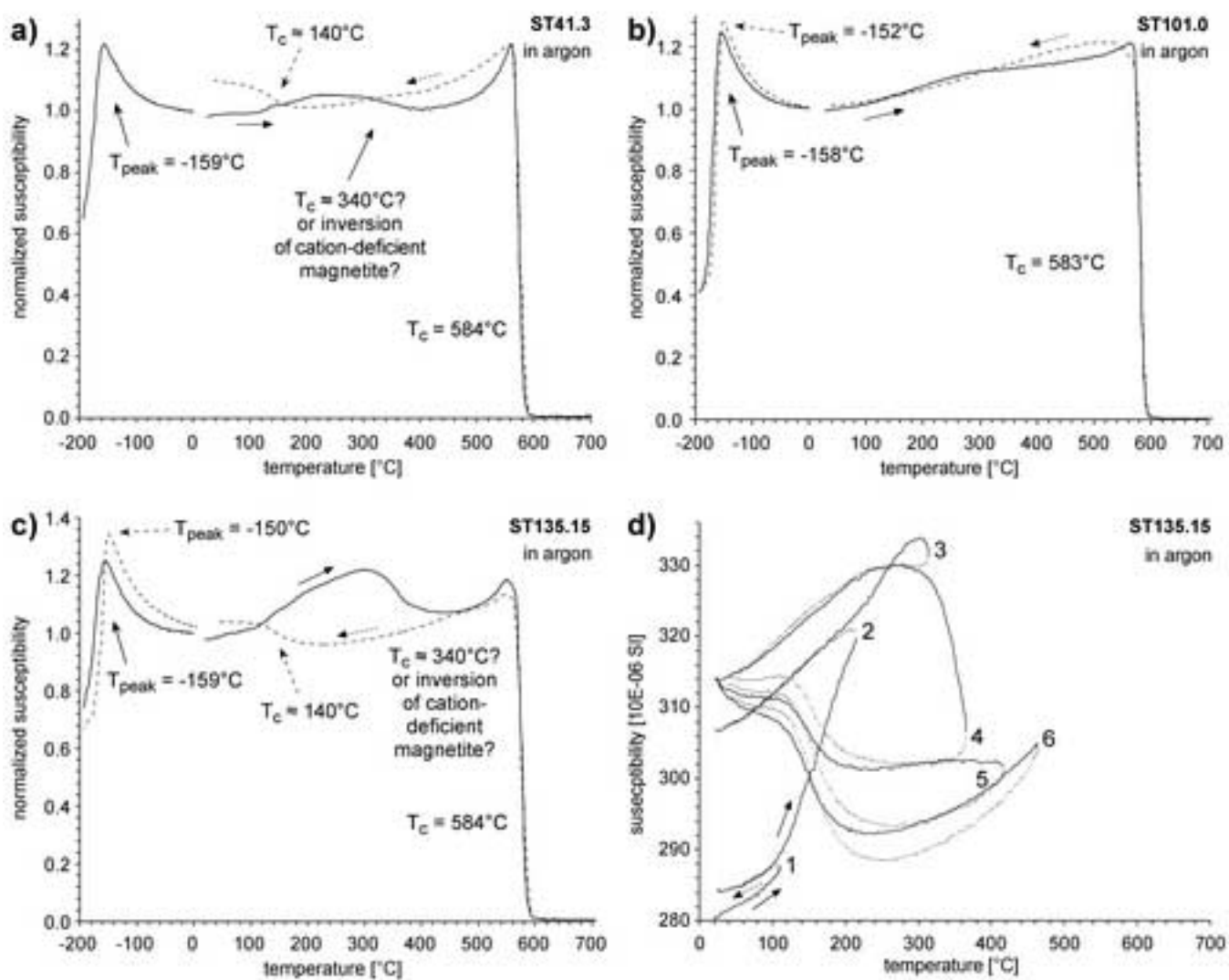


Fig. 9

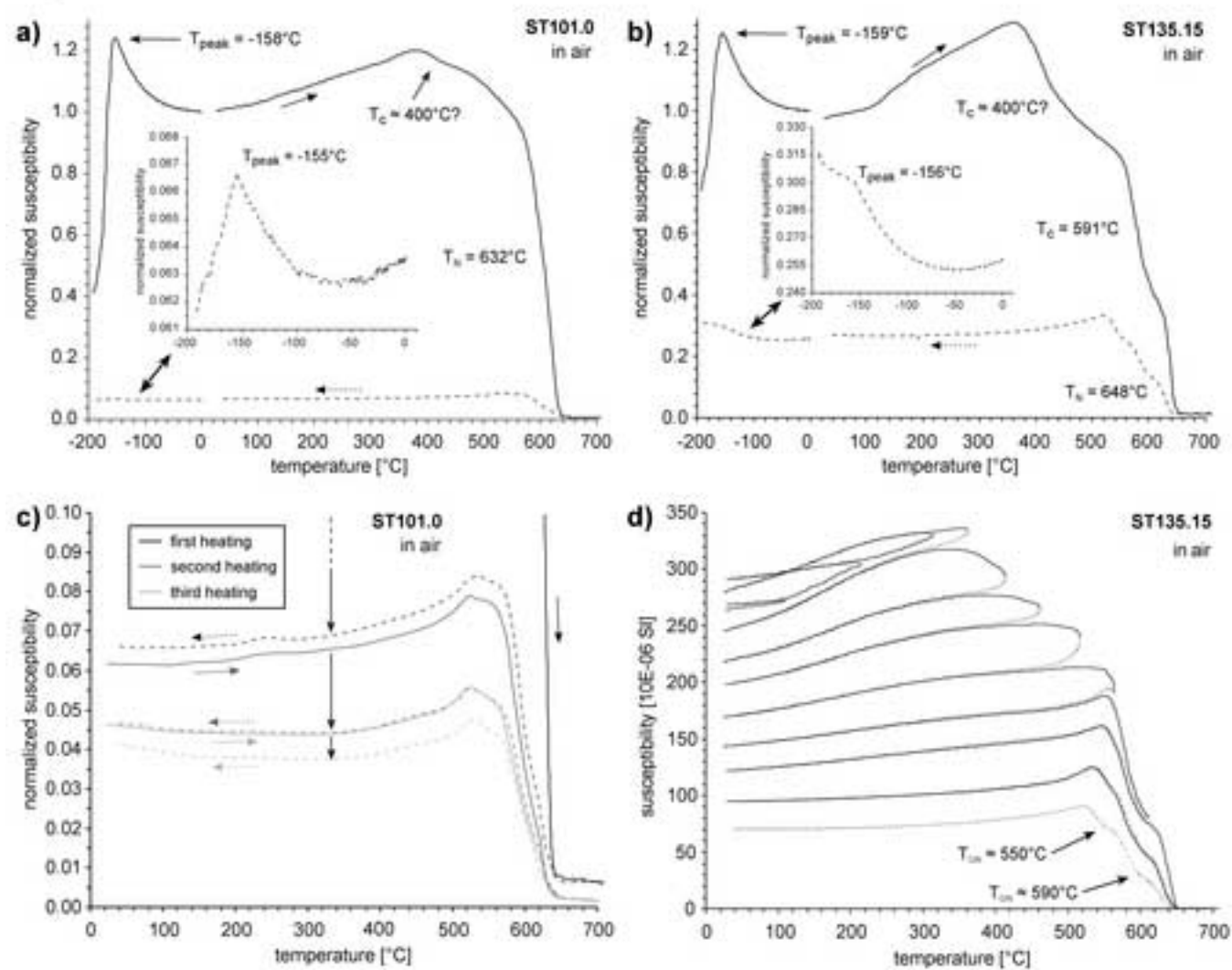


Fig. 10

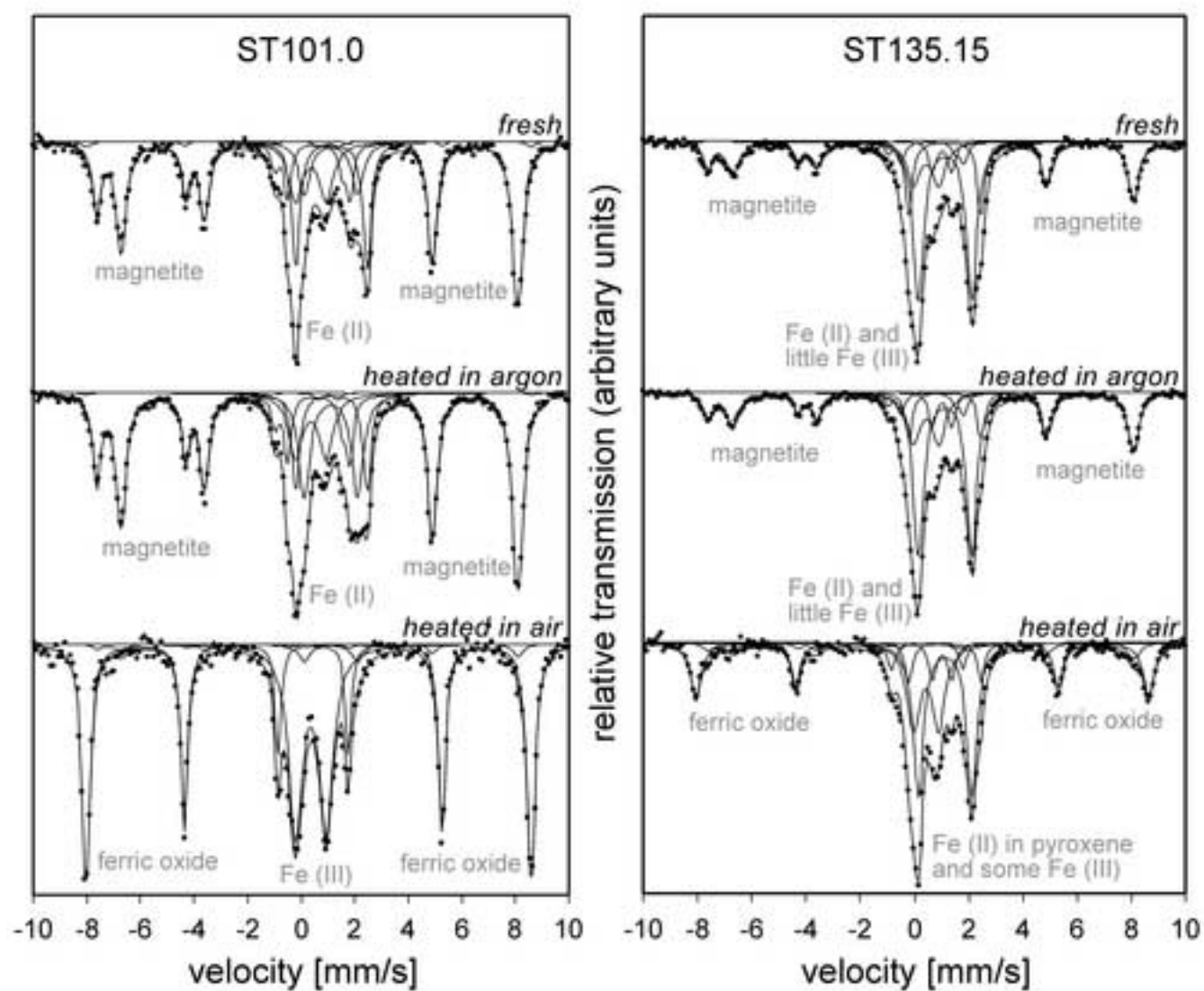


Fig. 11

